The Journal of Chemical Physics

The four-component DFT method for the calculation of the EPR g-tensor using a restricted magnetically balanced basis and London atomic orbitals

Cite as: J. Chem. Phys. **157**, 164114 (2022); https://doi.org/10.1063/5.0103928
Submitted: 17 June 2022 • Accepted: 27 September 2022 • Accepted Manuscript Online: 28 September 2022 • Published Online: 31 October 2022

Debora Misenkova, Florian Lemken, Michal Repisky, et al.

View Online Export Citation CrossMark

ARTICLES YOU MAY BE INTERESTED IN

Multiconfigurational short-range density functional theory for nuclear magnetic resonance shielding constants with gauge-including atomic orbitals
The Journal of Chemical Physics **157**, 164106 (2022); https://doi.org/10.1063/5.0106422

Exact two-component Hamiltonians for relativistic quantum chemistry: Two-electron picture-change corrections made simple
The Journal of Chemical Physics **157**, 114106 (2022); https://doi.org/10.1063/5.0095112

4-component relativistic Hamiltonian with effective QED potentials for molecular calculations
The Journal of Chemical Physics **157**, 164101 (2022); https://doi.org/10.1063/5.0116140

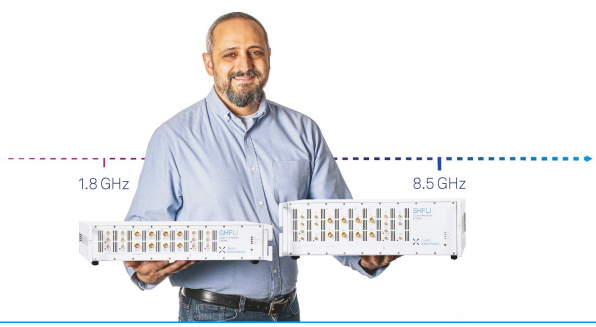

Trailblazers. New
Meet the Lock-in Amplifiers that measure microwaves.
Zurich Instruments
Find out more

© 2022 Author(s).

AIP Publishing

The Journal of Chemical Physics ARTICLE scitation.org/journal/jcp

The four-component DFT method for the calculation of the EPR g-tensor using a restricted magnetically balanced basis and London atomic orbitals

Cite as: J. Chem. Phys. 157, 164114 (2022); doi: 10.1063/5.0103928
Submitted: 17 June 2022 • Accepted: 27 September 2022 •
Published Online: 31 October 2022

View Online Export Citation CrossMark

Debora Misenkova,[1] Florian Lemken,[1] Michal Repisky,[2,3] Jozef Noga,[4] Olga L. Malkina,[1] and Stanislav Komorovsky[1,4,a)]

AFFILIATIONS

[1] Institute of Inorganic Chemistry, Slovak Academy of Sciences, Dúbravská cesta 9, SK-84536 Bratislava, Slovakia
[2] Hylleraas Centre for Quantum Molecular Sciences, Department of Chemistry, UiT–The Arctic University of Norway, N-9037 Tromsø, Norway
[3] Department of Physical and Theoretical Chemistry, Faculty of Natural Sciences, Comenius University, Ilkovicova 6, SK-84215 Bratislava, Slovakia
[4] Department of Inorganic Chemistry, Faculty of Natural Sciences, Comenius University, Ilkovicova 6, SK-84215 Bratislava, Slovakia

[a)] **Author to whom correspondence should be addressed:** stanislav.komorovsky@savba.sk

ABSTRACT

Four-component relativistic treatments of the electron paramagnetic resonance g-tensor have so far been based on a common gauge origin and a restricted kinetically balanced basis. The results of such calculations are prone to exhibit a dependence on the choice of the gauge origin for the vector potential associated with uniform magnetic field and a related dependence on the basis set quality. In this work, this gauge problem is addressed by a distributed-origin scheme based on the London atomic orbitals, also called gauge-including atomic orbitals (GIAOs), which have proven to be a practical approach for calculations of other magnetic properties. Furthermore, in the four-component relativistic domain, it has previously been shown that a restricted magnetically balanced (RMB) basis for the small component of the four-component wavefunctions is necessary for achieving robust convergence with regard to the basis set size. We present the implementation of a four-component density functional theory (DFT) method for calculating the g-tensor, incorporating both the GIAOs and RMB basis and based on the Dirac–Coulomb Hamiltonian. The approach utilizes the state-of-the-art noncollinear Kramers-unrestricted DFT methodology to achieve rotationally invariant results and inclusion of spin-polarization effects in the calculation. We also show that the gauge dependence of the results obtained is connected to the nonvanishing integral of the current density in a finite basis, explain why the results of cluster calculations exhibit surprisingly low gauge dependence, and demonstrate that the gauge problem disappears for systems with certain point-group symmetries.

Published under an exclusive license by AIP Publishing. https://doi.org/10.1063/5.0103928

I. INTRODUCTION

Analysis of the g-tensor, one of the parameters of electron paramagnetic resonance (EPR) spectroscopy, is an important tool in characterizing the electronic structure of open-shell systems. The usefulness of EPR parameters is further increased by the fact that EPR tensors can be used to study the Curie contribution to the nuclear magnetic resonance (NMR) parameters of a paramagnetic species.[1–3] When heavy atoms are present in the system, the quality of the relativistic computational methodology becomes very important in the prediction of the components of the g-tensor. For this reason, relativistic methods based on density functional theory (DFT) that include spin–orbit effects variationally (self-consistently) are becoming increasingly popular for the calculation of EPR parameters (see, for example, Refs. 4–18). One reason for their popularity is that these methods combine the computational

Published under an exclusive license by AIP Publishing

efficiency of DFT with the accuracy of four- or two-component relativistic theories. Besides the efficient inclusion of correlation effects by DFT approaches, the quality of these methodologies stands on three pillars: (1) the treatment of relativistic effects in general and spin–orbit effects in particular; (2) the quality of the DFT approaches used, i.e., the inclusion of spin-polarization effects and the usage of noncollinear exchange–correlation (xc) functionals; (3) the quality of the basis sets, i.e., a proper balance of the large- and small-component basis, and use of a gauge-origin-dependent basis in order to enforce the gauge origin independence of the result.

The difference between the g-tensor and the free electron g-value, the g-shift, is mainly caused by spin–orbit (SO) interaction. The prediction of the g-shift for systems that contain only light elements, e.g., organic radicals, usually requires only the inclusion of linear SO effects in the calculation. However, even in this case, one should consider more accurate relativistic methodologies because there are cases of systems containing relatively light elements for which higher-order SO contributions become important (see, for example, the quadratic SO contribution to the g-shift in the SeO molecule in Ref. 5). In the case of systems containing heavy elements, the importance of higher-order SO effects should not be underestimated[11] and the variational inclusion of relativistic effects becomes necessary. The implementation of (one-electron) nuclear SO effects variationally is straightforward and computationally undemanding. In contrast, computationally efficient inclusion of the (two-electron) spin-same-orbit (SSO) and spin-other-orbit (SOO) interactions[19] is a more challenging task. Fortunately, the SOO contributions are relatively more important in the calculations of systems that contain only light elements than for heavy-element-containing systems.[16,20] As a result, methods that are based on the Dirac–Coulomb Hamiltonian, and thus omit the SOO terms, provide a reasonable compromise between precision and computational efficiency when predicting g-tensor parameters of heavy-element-containing systems.

Another issue related to that of inclusion of higher-order spin–orbit effects in the calculation is the restriction of current DFT methodologies to the calculation of those magnetic parts of the EPR effective-spin Hamiltonian that are only linear in the spin operators.[21] The effective Hamiltonian that contains only linear terms for description of the electronic Zeeman and hyperfine interactions can only properly describe magnetic interactions of systems with higher than triplet multiplicity, $S > 1$, when higher-than-linear SO effects can be safely neglected.[22] On the other hand, for systems where only two or three electronic states are populated, there is no such restriction, and this type of effective Hamiltonian properly describes systems with arbitrary-strength SO interactions of any order.[22] Therefore, those DFT approaches that aim to include higher-order SO effects are currently only suitable for the treatment of systems with doublet or triplet multiplicity.

Upon the incorporation of spin–orbit effects into the Hamiltonian, the exchange–correlation energy of open-shell species derived from nonrelativistic (nr) xc functionals becomes dependent on the rotation of the Cartesian coordinate axis system. This unphysical behavior is a result of the reliance of nr xc functionals on the quantization axis that defines alpha and beta densities and of the coupling of spatial and spin degrees of freedom mediated by the SO interaction. This class of xc functionals is often referred to as collinear. Although the ideal solution to this problem would be to use genuine relativistic noncollinear xc functionals, so far only limited work has been done on their development.[23–27] Nowadays the preservation of the rotational invariance of the xc energy is usually accomplished by the introduction of the noncollinear variables into the definition of the nr xc functionals. For example, the collinear variable ρ_z, the z component of the spin density, is substituted by the length of the spin density vector $|\vec{\rho}|$ in noncollinear approaches. Interested readers can find more details on the development of noncollinear xc functionals for open-shell systems in Refs. 17, 21, and 28–33 and the works cited therein. In particular, we note the problem of numerical instabilities that arise when the spin density approaches zero in the noncollinear xc potentials and kernels that involve gradient variables, discussion of which may be found in Refs. 31 and 32. In this work, we employ the noncollinear ansatz of Scalmani and Frisch[31] with the regularization of xc potentials and kernels presented in Ref. 32. The quality of the noncollinear DFT methodology is also closely related to the quality of the Kohn–Sham (KS) determinant. Nowadays, state-of-the-art DFT methodology utilizes a Kramers-unrestricted KS determinant to account for the important spin-polarization effects. In contrast, the DFT methods based on Kramers-restricted KS determinants neglect spin-polarization effects, leading to unsatisfactory results, especially in the case of hyperfine coupling constants.[34]

Without special measures, calculations of molecular properties that depend on a uniform external magnetic field are plagued by the gauge dependence of the results. This dependence vanishes in the complete basis set limit; thus, the gauge dependence problem can be mitigated by using sufficiently saturated basis sets. However, there also exist well-established methods that provide reliable results without the need for imposing additional significant requirements on the basis set size. The most popular methods in this respect are the ones that use gauge-including atomic orbitals (GIAOs), also known as London atomic orbitals (LAOs).[35,36] The success of the GIAO-based approaches is due less to the formal gauge independence of the results themselves than to the fast convergence of the results with the basis set size. The use of GIAOs shifts part of the burden of describing the magnetic field dependence of the wavefunctions from the molecular orbital coefficients to the atomic orbital basis itself, which ultimately decreases the basis set requirements. In the nonrelativistic case of a hydrogen-like system, the LAOs properly describe the first-order response of the wavefunction with respect to a uniform external magnetic field. In the relativistic case, the LAOs provide a correct description of the first-order response up to order c^{-2}, see also the discussion in Ref. 37.

In addition, when developing four-component methods for the calculation of molecular properties that involve magnetic fields, one must pay special attention to proper magnetic balance between the basis of the small and large components of the four-component wavefunction. Moreover, for the four-component calculation of second-order magnetic properties, the inclusion of magnetically balanced basis is absolutely necessary. The most relevant approaches include the so-called Kutzelnigg transformation,[38] the restricted magnetically balanced basis (RMB),[37,39–41] and the simple magnetic balance,[42,43] (we refer the interested reader to a more detailed discussion of the magnetically balanced bases in Ref. 44). In this work,

Published under an exclusive license by AIP Publishing

we will utilize the RMB approach as it allows the calculation of both NMR shielding[37,39,40] and indirect spin–spin coupling tensors.[41] To summarize, one can safely assume that the combination of an RMB basis with GIAOs for the calculation of the g-tensor within the four-component framework is expected to exhibit robust convergence with the basis set size.

There is evidence that the gauge dependence of the calculated results is usually less severe for the g-tensor than for other magnetic properties—such as, for example, the NMR shielding tensor.[4,20,45–48] However, there are instances where the gauge dependence of the g-tensor calculations becomes noticeable and warrants the development of methods that address the issue, see Refs. 4 and 49–52 and the discussion in Ref. 52. Glasbrenner *et al.*[52] noticed that in many cases, the somewhat smaller gauge dependence of g-tensor calculations "can also be explained by the fact that most previous studies focused on g-tensors of small molecules." However, we have also found this to be the case for some systems containing a single heavy element, regardless of the system size (see, for example, Ref. 48). As explained below, in such a case, the negligible gauge dependence of the g-tensor is connected to the symmetry of the immediate electronic environment of the heavy atom. In other cases, even small systems can exhibit strong gauge dependence of the results when one moves the gauge away from the molecular center.[4,49,52] However, such gauge choices are artificial and chosen only to make the point; in practical applications, one would use a well-defined molecular gauge (e.g., the center of nuclear charge of the molecule, the center of mass of the molecule, or the center of the electron spin density, among others),[52] which, as mentioned above, usually leads to rather small gauge dependence of the results. There are, however, situations where choosing an optimal position of the gauge is not possible. The most obvious example is that of solid-state (periodic) calculations, in which the computational methodologies must be based on distributed gauge origin methods (such as GIAO methods), as potentials dependent on a single gauge origin are not periodic. In single molecule calculations, the choice of the gauge becomes problematic if multiple spin centers are present in the system. A special case of these is that of so-called "molecular-cluster computations," which are used as an approximation to solid-state calculations.[53]

Although the development of DFT methodologies for g-tensor calculations has a long history (see, for example, Refs. 4, 9, 20, and 54–59 and the works cited therein), the development and implementation of noncollinear DFT approaches that include spin–orbit effects variationally is rather rare.[5,16,18,60] From this list, only the work of Franzke and Yu[18] tackles the gauge dependence of the results at all, with the authors employing GIAOs. All four of the noncollinear DFT methodologies just mentioned include the full nuclear SO interaction, but they include the two-electron SO interaction (SSO and SOO contributions) at various levels of theory that usually involve some approximation to the full Coulomb–Breit electron–electron interaction. The authors of the two-component methodologies presented in Refs. 5 and 16 approximate SSO and SOO terms by means of the atomic-mean field approach,[61,62] while in Refs. 16 and 18, the SSO contribution is modeled by scaling the nuclear SO term[63,64] and the SOO contribution is neglected. The four-component method developed in Ref. 60 is based on the Dirac–Coulomb Hamiltonian and, thus, includes the SSO contribution, while the SOO interaction is omitted as it is a part of the Gaunt electron–electron interaction.[19] All four methodologies[5,16,18,60] take advantage of the noncollinear reformulation of the otherwise collinear nr xc functionals to make the calculated results rotationally invariant. However, in order to take into account the gradient variables that are necessary to utilize functionals beyond local-density approximation, the noncollinear ansatz used is derived from the gradient of the length of the spin density, $\vec{\nabla}|\vec{\rho}\,|$ (see, for example, Refs. 33 and 65). As a result, some of the terms appearing in the xc potential exhibit numerical instabilities.[31,32] In Refs. 5 and 60, these unstable terms are simply neglected, which makes the xc potential non-variational with respect to the xc energy, but the expressions become numerically stable [see Eq. (68) and the corresponding discussion in Ref. 17]. On the other hand, the authors of Refs. 16 and 18 use the noncollinear methodology as presented in Ref. 66, where it is not clear if the numerical instabilities have been avoided by neglecting unstable terms as done in Refs. 5, 33, and 60, or by using a large cutoff threshold as done in Ref. 65, or by other methods—or if they have been avoided at all.

The goal of this work is to provide a state-of-the-art methodology that addresses all the points discussed above as follows: (1) It treats the relativistic effects variationally and is based on the Dirac–Coulomb Hamiltonian; (2) it includes spin-polarization effects by means of the Kramers-unrestricted KS determinant, and it utilizes noncollinear regularized xc functionals; (3) it takes advantage of the London atomic orbitals as well as a restricted magnetically balanced basis when constructing the small component of the four-component wavefunction. The presented approach thus aims to provide both a benchmark methodology for the development of more approximate relativistic methods and a robust way to predict the g-tensor in routine applications.

In Secs. III–V, we present the four-component theory for calculating the g-tensor using the RMB–GIAO, restricted kinetically balanced, and restricted magnetically balanced bases, respectively. Section VI contains the computational details of our calculations, which are then presented in Sec. VII. In Sec. VII, we discuss the convergence of the g-tensor results with the basis set size, the use of the double point-group symmetry in estimation of the g-tensor gauge dependence, and the surprisingly weak gauge dependence of the results in the molecular-cluster calculations. In Sec. VIII, we present our concluding remarks. Finally, in Appendixes A and B, we prove the continuity equation within the framework of the Dirac–Kohn–Sham theory as well as an important consequence thereof: the vanishing integral of the current density.

II. NOTATION

Throughout this work, we use the Hartree system of atomic units. Thus, for example, the Bohr magneton has the value $\frac{1}{2c}$, with c being the speed of light in atomic units. Summation over repeated indices is assumed unless stated otherwise. Indices i, j denote occupied positive-energy molecular orbitals, u, v, and k denote Cartesian components, m and n represent components of the four-component vector $1,\ldots,4$, and η represents the scalar atomic orbital basis. In addition, we employ flattened atomic orbital indices μ, ν, which combine the four-component and atomic orbital indices, $\mu := m\eta$ (see also the discussion in Ref. 32). Unless stated otherwise, bold font indicates a matrix whose dimension is defined in the text.

Published under an exclusive license by AIP Publishing

III. CALCULATION OF THE g-TENSOR USING AN RMB–GIAO BASIS

Within the framework of Kramers-unrestricted (KU) Hartree–Fock (HF) and density functional theory (DFT), components of the g-tensor can be calculated as[5,21,60]

$$g_{uv} = \frac{2c}{S}\frac{dE(\vec{J}_v,\vec{B})}{dB_u}\bigg|_{\vec{B}=0}, \tag{1}$$

where $\vec{J}_v$ is the magnetization vector of the vth Kohn–Sham (KS) determinant, and S is the effective spin of the system. The formal multiplicity of the system, $2S+1$, is equal to the number of populated states, i.e., the number of electronic states that are described by the EPR effective-spin Hamiltonian.[21,67] Each of the three orthogonal magnetization vectors corresponds to a separate KS determinant, which is in practice obtained from an independent self-consistent calculation (see also the discussion in Ref. 21). The elements of the g-tensor are then obtained as the first-order derivative of the total electronic energy E with respect to an external uniform magnetic field $\vec{B}$. In the Coulomb gauge, the vector potential corresponding to this magnetic field has the form

$$\vec{A} = \frac{1}{2}(\vec{B}\times\vec{r}_G), \qquad \vec{r}_G = \vec{r}-\vec{r}_0, \tag{2}$$

where $\vec{r}_0$ is the position of the gauge origin and $\vec{r}$ is the position vector of the electron. Within the Dirac–Hartree–Fock (DHF) and Dirac–Kohn–Sham (DKS) formalisms, the minimal coupling substitution, $\vec{p}\to\vec{p}+\frac{1}{c}\vec{A}$, is used to obtain the electronic energy of a system in the presence of an external magnetic field,

$$E(\vec{J}_v,\vec{B}) = \langle\varphi_i(\vec{J}_v,\vec{B})|h(\vec{B})|\varphi_i(\vec{J}_v,\vec{B})\rangle + E^{2e}(\vec{J}_v,\vec{B}), \tag{3}$$

$$\mathbf{h}(\vec{B}) = c\vec{\boldsymbol{\alpha}}\cdot\vec{p} + \vec{\boldsymbol{\alpha}}\cdot\vec{A} + (\boldsymbol{\beta}-\mathbf{I}_4)c^2 - V^{\mathrm{nuc}}(\vec{r})\mathbf{I}_4, \tag{4}$$

$$E^{2e}(\vec{J}_v,\vec{B}) = E^{\mathrm{ee}}(\vec{J}_v,\vec{B}) - \xi E^{\mathrm{ex}}(\vec{J}_v,\vec{B}) + E^{\mathrm{xc}}[\vec{J}_v,\vec{B},(1-\xi)]. \tag{5}$$

Here, $\boldsymbol{\beta}$ and $\vec{\boldsymbol{\alpha}}$ are the 4×4 Dirac matrices given by

$$\boldsymbol{\beta} = \begin{pmatrix}\mathbf{I}_2 & \mathbf{0}_2\\ \mathbf{0}_2 & -\mathbf{I}_2\end{pmatrix}, \qquad \vec{\boldsymbol{\alpha}} = \begin{pmatrix}\mathbf{0}_2 & \vec{\boldsymbol{\sigma}}\\ \vec{\boldsymbol{\sigma}} & \mathbf{0}_2\end{pmatrix}, \tag{6}$$

where $\vec{\boldsymbol{\sigma}}$ is a vector constructed from the Pauli matrices,

$$\boldsymbol{\sigma}_1 = \begin{pmatrix}0 & 1\\ 1 & 0\end{pmatrix}, \qquad \boldsymbol{\sigma}_2 = \begin{pmatrix}0 & -\mathrm{i}\\ \mathrm{i} & 0\end{pmatrix}, \qquad \boldsymbol{\sigma}_3 = \begin{pmatrix}1 & 0\\ 0 & -1\end{pmatrix}, \tag{7}$$

and $\mathbf{I}_n$ ($\mathbf{0}_n$) is the $n\times n$ identity (zero) matrix. The dependence on the magnetization vector and the external magnetic field is denoted by $(\vec{J}_v,\vec{B})$. The parameter ξ represents the admixture of the HF exact exchange: $\xi=1$ corresponds to pure HF theory, $\xi=0$ to pure DFT, and $0<\xi<1$ to hybrid theories. $V^{\mathrm{nuc}}(\vec{r})$ is the scalar electrostatic potential due to fixed atomic nuclei. The presence of heavy nuclei and the four-component relativistic framework necessitates the use of a finite model for the nuclear charge distribution.[68] In this work, we use an s-type Gaussian function to describe the finite-size nuclear charge distribution (for detailed expressions, see Ref. 17). The two-electron potential energy, Eq. (5), consists of the Coulomb energy E^{ee}, Hartree–Fock exchange energy E^{ex}, and exchange–correlation energy E^{xc},

$$E^{\mathrm{ee}} = \frac{1}{2}\iint\frac{\varphi^*_{mi}(\vec{r}_1)\varphi_{mi}(\vec{r}_1)\varphi^*_{nj}(\vec{r}_2)\varphi_{nj}(\vec{r}_2)}{|\vec{r}_1-\vec{r}_2|}d^3\vec{r}_1d^3\vec{r}_2, \tag{8}$$

$$E^{\mathrm{ex}} = \frac{1}{2}\iint\frac{\varphi^*_{mi}(\vec{r}_1)\varphi_{mj}(\vec{r}_1)\varphi^*_{nj}(\vec{r}_2)\varphi_{ni}(\vec{r}_2)}{|\vec{r}_1-\vec{r}_2|}d^3\vec{r}_1d^3\vec{r}_2, \tag{9}$$

$$E^{\mathrm{xc}} = \int\varepsilon^{\mathrm{xc}}\left[\rho_0,\vec{\nabla}\rho_0,\vec{\rho},\vec{\nabla}\vec{\rho}\right]d^3\vec{r}, \tag{10}$$

where for the sake of simplicity, we have dropped the dependence on the magnetic field and the magnetization vector from the MOs, $\varphi_{mj}(\vec{r}_1) := \varphi_{mj}(\vec{r}_1,\vec{J}_v,\vec{B})$. In Eq. (10), $\varepsilon^{\mathrm{xc}}$ represents the exchange–correlation energy density that depends within the generalized-gradient approximation on the charge and spin densities and their gradients,

$$\rho_l(\vec{J}_v,\vec{B}) = \varphi^*_{mi}(\vec{J}_v,\vec{B})\,(\Sigma_l)_{mn}\,\varphi_{ni}(\vec{J}_v,\vec{B}), \tag{11}$$

$$\boldsymbol{\Sigma}_l = \begin{pmatrix}\boldsymbol{\sigma}_l & \mathbf{0}_2\\ \mathbf{0}_2 & \boldsymbol{\sigma}_l\end{pmatrix}, \qquad l=0,\ldots,3, \tag{12}$$

with $\boldsymbol{\sigma}_0 := \mathbf{I}_2$. Methods that include spin–orbit effects variationally must employ the so-called noncollinear ansatz for the nr exchange–correlation functionals (see also the discussion at the end of this section). We refer the interested reader to Ref. 17 for a detailed discussion of the implementation of both the perturbation-free and the linear-response two-electron contributions to the energy and potentials used in this work [see also Eqs. (27)–(29)].

The four-component molecular orbitals (MOs) φ_{mi} are expanded in a finite set of four-component basis functions that combine the GIAOs and the RMB basis for the small component of the MO as follows[17,37] (η is not a summation index),

$$\varphi_{mi}(\vec{r},\vec{J}_v,\vec{B}) = X^{\mathrm{RMB-GIAO}}_{m\mu}(\vec{r},\vec{B})C_{\mu i}(\vec{J}_v,\vec{B}), \tag{13}$$

$$X^{\mathrm{RMB-GIAO}}_{mn\eta}(\vec{r},\vec{B}) = \mathcal{O}^{\mathrm{RMB}}_{mn}\,\omega_\eta(\vec{r},\vec{B})\,\chi_\eta(\vec{r}), \tag{14}$$

$$\mathcal{O}^{\mathrm{RMB}} = \begin{pmatrix}\mathbf{I}_2 & \mathbf{0}_2\\ \mathbf{0}_2 & \frac{1}{2c}\vec{\boldsymbol{\sigma}}\cdot\left(\vec{p}+\frac{1}{c}\vec{A}\right)\end{pmatrix}, \tag{15}$$

where $\mu := n\eta$ and $\chi_\eta(\vec{r})$ is a scalar basis function. In Eq. (13), the molecular orbital coefficients $C_{\mu i}(\vec{J}_v,\vec{B})$ are the solutions of the Fock equation in the presence of a magnetic field $\vec{B}$, where the Fock matrix is obtained as the derivative of the energy given in Eq. (3) with respect to the density matrix (see, for example, Refs. 17 and 32). In Eq. (14), we apply London orbitals in the framework of the four-component theory using the approach presented in Ref. 37, where the phase factor ω_η, which ensures energy invariance with respect to the change of the gauge origin $\vec{r}_0$, has the form

$$\omega_\eta(\vec{r},\vec{B}) = \exp\left\{\frac{-i}{2c}\left[\vec{B}\times\left(\vec{R}_\eta-\vec{r}_0\right)\right]\cdot\vec{r}\right\}. \tag{16}$$

Published under an exclusive license by AIP Publishing

Here, $\vec{R}_\eta$ is the position of the nucleus at which the atomic orbital χ_η is centered. The function $\omega_\eta\chi_\eta$ is known as a London atomic orbital.[35] Because the four-component basis functions, Eq. (14), have an explicit dependence on the perturbation parameters $\vec{B}$, it is useful to follow the perturbation theory formalism based on the Lagrange functional. This allows us to take advantage of the variational conditions imposed on the Lagrangian and simplify the expression for the energy derivative (for more details see, for example, Refs. 69 and 70). By employing the perturbation-dependent basis, $X_{m\mu}$, the g-tensor can then be expressed as

$$g_{uv} = \frac{2c}{S}\left[\frac{\partial L_v}{\partial B_u} + \frac{\partial L_v}{\partial X_{m\mu}}\frac{dX_{m\mu}}{dB_u} + \frac{\partial L_v}{\partial X^*_{m\mu}}\frac{dX^*_{m\mu}}{dB_u}\right]\Bigg|_{\vec{B}=0}, \tag{17}$$

where $\partial/\partial\lambda$ and $d/d\lambda$ denote the partial and total derivatives with respect to the variable λ, respectively. The Lagrange functional L_v is constructed from the electronic energy in Eq. (3) and the orthonormality constraints on the molecular orbitals as follows [here and in Eq. (19), v is not a summation index]:

$$\begin{aligned} L_v &:= L\big[\vec{B}, X(\vec{B}), C(\vec{J}_v,\vec{B}), \varepsilon(\vec{J}_v,\vec{B})\big] \\ &= E\big[\vec{B}, X(\vec{B}), C(\vec{J}_v,\vec{B})\big] - \varepsilon_i(\vec{J}_v,\vec{B}) \\ &\quad\times\Big[\mathbf{C}_i^\dagger(\vec{J}_v,\vec{B})\,\mathbf{S}(X)\,\mathbf{C}_i(\vec{J}_v,\vec{B}) - 1\Big]. \end{aligned} \tag{18}$$

Here, the overlap matrix in the RMB–GIAO basis has the form $S_{\mu\nu} = \langle X_\mu^{\text{RMB–GIAO}} | X_\nu^{\text{RMB–GIAO}}\rangle$ and the bold font on MO coefficients, $\mathbf{C}_i$, indicates that the ith molecular orbital is a vector, $C_{\mu i}$. Combining Eqs. (17) and (18) then leads to the following expression for the g-tensor:

$$g_{uv} = \frac{2c}{S}\mathbf{C}_i^\dagger(\vec{J}_v,0)\big[\mathbf{h}^{B_u} - \mathbf{S}^{B_u}\varepsilon_i(\vec{J}_v,0) + \mathbf{V}^{2\,e,B_u}(\vec{J}_v,0)\big]\mathbf{C}_i(\vec{J}_v,0), \tag{19}$$

$$\begin{aligned} h^{B_u}_{\mu\nu} &= \langle X_\mu^{B_u}|h(0)|X_\nu^{\text{RKB}}\rangle + \langle X_\mu^{\text{RKB}}|h(0)|X_\nu^{B_u}\rangle \\ &\quad + \frac{1}{2}\langle X_\mu^{\text{RKB}}|(\vec{r}_G\times\vec{\alpha})_u|X_\nu^{\text{RKB}}\rangle, \end{aligned} \tag{20}$$

$$S^{B_u}_{\mu\nu} = \langle X_\mu^{B_u}|X_\nu^{\text{RKB}}\rangle + \langle X_\mu^{\text{RKB}}|X_\nu^{B_u}\rangle, \tag{21}$$

$$X^{B_u}_{m\mu} = \frac{dX^{\text{RMB–GIAO}}_{m\mu}}{dB_u}\Bigg|_{\vec{B}=0}, \tag{22}$$

with the restricted kinetically balanced (RKB) basis[71,72] defined as $\mathbf{X}^{\text{RKB}} = \mathbf{X}^{\text{RMB–GIAO}}(\vec{B}=0)$. For the sake of simplicity, in the following, we omit the explicit dependence on $(\vec{J}_v,0)$ of the MO coefficients, one-electron energies, and two-electron potentials. The MO coefficients $C_{\mu i}$ and one-electron energies ε_i are the solutions of the perturbation-free Fock equation, i.e.,

$$\mathbf{FC} = \mathbf{SC}\boldsymbol{\varepsilon}, \tag{23}$$

$$F_{\mu\nu} = \langle X_\mu^{\text{RKB}}|h(0)|X_\nu^{\text{RKB}}\rangle + V^{2e,0}_{\mu\nu}, \tag{24}$$

$$S_{\mu\nu} = \langle X_\mu^{\text{RKB}}|X_\nu^{\text{RKB}}\rangle, \tag{25}$$

with the two-electron perturbation-free potential, $\mathbf{V}^{2e,0}$, as defined, for example, in Ref. 32. In Eq. (19), the two-electron contribution, $\mathbf{V}^{2\,e,B_u}$, consists of the Coulomb, HF exact exchange, and exchange–correlation terms,

$$\mathbf{V}^{2e,B_u} = \mathbf{V}^{\text{ee},B_u} - \xi\mathbf{V}^{\text{ex},B_u} + \mathbf{V}^{\text{xc},B_u}[1-\xi], \tag{26}$$

$$\mathbf{V}^{\text{ee},B_u} = \iint \frac{\text{Tr}\{\boldsymbol{\Omega}^{0,\text{RKB}}(\vec{r}_1)\,\mathbf{D}\}\boldsymbol{\Omega}^{0,B_u}(\vec{r}_2)}{|\vec{r}_1-\vec{r}_2|}d^3\vec{r}_1\,d^3\vec{r}_2, \tag{27}$$

$$\mathbf{V}^{\text{ex},B_u} = \iint \frac{\boldsymbol{\Omega}^{0,\text{RKB}}(\vec{r}_1)\,\mathbf{D}\,\boldsymbol{\Omega}^{0,B_u}(\vec{r}_2)}{|\vec{r}_1-\vec{r}_2|}d^3\vec{r}_1\,d^3\vec{r}_2, \tag{28}$$

$$\mathbf{V}^{\text{xc},B_u} = \int\Big[f_l\,\boldsymbol{\Omega}^{l,B_u}(\vec{r}) + \tilde{f}_{lk}\nabla_k\boldsymbol{\Omega}^{l,B_u}(\vec{r})\Big]d^3\vec{r}. \tag{29}$$

In the above equations for the response two-electron potentials, the density matrix $\mathbf{D}$ has the form

$$D_{\mu\nu} = C_{\mu i}C^*_{\nu i}, \tag{30}$$

and the overlap distributions are defined as

$$\Omega^{l,\text{RKB}}_{\mu\nu} = \big(X^{\text{RKB}}_{m\mu}\big)^*(\Sigma_l)_{mn}X^{\text{RKB}}_{n\nu}, \tag{31}$$

$$\Omega^{l,B_u}_{\mu\nu} = \big(X^{\text{RKB}}_{m\mu}\big)^*(\Sigma_l)_{mn}X^{B_u}_{n\nu} + \text{c.c.} \tag{32}$$

The implementation of the two-electron four-center integrals in the RMB–GIAO basis and their contraction with the density matrix, Eqs. (27) and (28), takes advantage of a novel formulation based on the complex quaternion algebra, which leads to a significant reduction of the computational cost when compared to standard algorithms.[17] The exchange–correlation contribution $\mathbf{V}^{\text{xc},B_u}$ is given by the derivatives of the exchange–correlation energy density ε^{xc},

$$f_l = \frac{\partial\varepsilon^{\text{xc}}}{\partial w_t}\frac{dw_t}{d\rho_l}, \qquad \tilde{f}_{kl} = \frac{\partial\varepsilon^{\text{xc}}}{\partial w_t}\frac{dw_t}{d(\nabla_k\rho_l)}, \tag{33}$$

where the perturbation-free charge density ρ_0 and spin density $\vec{\rho}$ have the form

$$\rho_l = \text{Tr}\{\boldsymbol{\Omega}^{l,\text{RKB}}\mathbf{D}\} \tag{34}$$

and $\{w_t\}$ represents a set of noncollinear variables. In this work, we use the set first proposed by Scalmani and Frisch.[31] To make the noncollinear xc potentials $\mathbf{V}^{\text{xc},0}$ and $\mathbf{V}^{\text{xc},B_u}$ numerically stable, we follow the regularization procedure first described in Ref. 32 in the framework of the four-component Kramers-unrestricted time-dependent DFT (KU-TDDFT) methodology. In this work, we have for the first time used this state-of-the-art noncollinear methodology in combination with the RMB–GIAO basis for the calculation of the EPR g-tensor.

IV. CALCULATION OF THE g-TENSOR USING AN RKB BASIS

When formulating perturbation theory on the basis of the Lagrange functional, one can choose either the MO coefficients or the MOs themselves as the variational parameters. In the former case, one formulates the theory in the finite basis from the start,

Published under an exclusive license by AIP Publishing

whereas in the latter case, the transition to the finite basis is made at a later stage of the derivation. The two different parametrizations lead to different sets of variational conditions,

$$\frac{dL_v}{dC^*_{\mu i}} = 0, \tag{35}$$

$$\frac{\delta L_v}{\delta \varphi^*_{mi}} = 0, \tag{36}$$

which, in the case of the perturbation-dependent basis, result in different working expressions for molecular properties. Conversely, if the basis does not depend on the perturbation parameters, the final expressions for both parametrizations are identical. The approach that defines the variational parameters as MO coefficients, is a more rigorous one, as it takes into account the finite nature of the basis from the start. The difference between the approaches vanishes in the complete basis; therefore, both approaches are valid if the provided finite basis is sufficiently large.

In Sec. III, we have used MO coefficients as the variational parameters, due to which the g-tensor expressions contain terms where the basis depends on the perturbation parameters, i.e., the second and third terms on the right-hand-side (RHS) of Eq. (17). To derive the final expressions for the g-tensor with the RKB basis, one option is to start from the RMB–GIAO expressions and remove terms that originate in the London phase factor [Eq. (16)] and the magnetic part of the RMB basis. Alternatively, one may use the MOs as variational parameters—as was done in Ref. 60—and, therefore, neither the London orbitals nor the magnetic part of the RMB basis would appear in the final working expression. Note in passing that the formulation of the response theory based on the MOs as variational parameters may prove advantageous as it simplifies the implementation of the indirect spin–spin coupling tensor[17] and helps to avoid possible divergences arising from the operator of the nuclear magnetic moment.[73]

In the following, we reformulate the theory for the calculation of the g-tensor presented in Ref. 60 in terms of the four-component current density. This formulation becomes useful later in the analysis of the molecular-cluster calculations and in double point-group symmetry considerations (see Sec. VII). The DKS expression for the g-tensor, which depends only on the gauge origin and the RKB basis, has the form (v is not a summation index)[60]

$$g_{uv} = \frac{2c}{S}\mathbf{C}_i^\dagger(\vec{J}_v,0)\,\mathbf{h}^{B_u,G}\,\mathbf{C}_i(\vec{J}_v,0), \tag{37}$$

$$h^{B_u,G}_{\mu\nu} = \frac{1}{2}\langle X^{\mathrm{RKB}}_\mu|(\vec{r}_G\times\vec{\alpha})_u|X^{\mathrm{RKB}}_\nu\rangle. \tag{38}$$

Using the expression for the four-component perturbation-free current density,

$$\vec{j}(\vec{J}_v,0) = -c\,\mathrm{Tr}\left\{\mathbf{X}^{\mathrm{RKB}\dagger}\vec{\alpha}\mathbf{X}^{\mathrm{RKB}}\mathbf{D}(\vec{J}_v,0)\right\}, \tag{39}$$

one can rewrite Eq. (37) as follows:

$$g_{uv} = -\frac{1}{S}\int\left[\vec{r}_G\times\vec{j}(\vec{J}_v,0)\right]_u d^3\vec{r}. \tag{40}$$

We refer the interested reader to other works[74,75] that use the current density in four-component theories of magnetic properties.

Equation (40) allows us to separate the gauge-dependent term in the expression for the g-tensor into two terms,

$$g_{uv} = -\frac{1}{S}\left\{\int\left[\vec{r}\times\vec{j}(\vec{J}_v,0)\right]_u d^3\vec{r} - \left[\vec{r}_0\times\int\vec{j}(\vec{J}_v,0)d^3\vec{r}\right]_u\right\}. \tag{41}$$

From this expression, one can deduce that the integral of the current density vanishes in a complete basis as the g-tensor results are gauge-independent in the basis set limit, i.e.,

$$\int\vec{j}(\vec{J}_v,0)d^3\vec{r} = 0. \tag{42}$$

Equation (42) follows from the continuity equation and the fact that in the static (time-independent) case, the number of electrons is constant in time in any closed volume. In Appendix A, we prove the continuity equation within the DKS theory and then use it in the proof of Eq. (42) in Appendix B. Interestingly, in pure DFT, $\xi = 0$, Eq. (42) holds for the current density generated by an individual MO (see Appendixes A and B).

V. CALCULATION OF THE g-TENSOR USING AN RMB BASIS

Following on from the discussion in Sec. IV, one can also devise a theory for g-tensor calculations by choosing the MO coefficients as the variational parameters and by selecting the RMB condition as the only dependence of the basis on the magnetic field, i.e., not considering the London orbitals. The EPR g-tensor expressions then depend on the gauge origin while also utilizing an RMB basis[39] for the small component of the four-component MOs,

$$\varphi_{mi}(\vec{r},\vec{J}_v,\vec{B}) = X^{\mathrm{RMB}}_{m\mu}(\vec{r},\vec{B})C_{\mu i}(\vec{J}_v,\vec{B}), \tag{43}$$

$$X^{\mathrm{RMB}}_{mn\eta}(\vec{r},\vec{B}) = \mathcal{O}^{\mathrm{RMB}}_{mn}\chi_\eta(\vec{r}), \tag{44}$$

where $\mu := n\eta$ and $\mathcal{O}^{\mathrm{RMB}}$ is defined in Eq. (15). The expressions for the calculation of the g-tensor then have formally the same form as the one presented in Sec. III [see Eq. (19)], where a RMB–GIAO basis was employed (v is not a summation index),

$$g_{uv} = \frac{2c}{S}\mathbf{C}_i^\dagger(\vec{J}_v,0)\left[\mathbf{h}^{B_u} - \mathbf{S}^{B_u}\varepsilon_i(\vec{J}_v,0) + \mathbf{V}^{2\,\mathrm{e},B_u}(\vec{J}_v,0)\right]\mathbf{C}_i(\vec{J}_v,0). \tag{45}$$

However, the different form of the RMB basis, compared to RMB–GIAO one, gives a different expression for $\mathbf{X}^{B_u}$,

$$X^{B_u}_{m\mu} = \left.\frac{dX^{\mathrm{RMB}}_{m\mu}}{dB_u}\right|_{\vec{B}=0}. \tag{46}$$

Then, to obtain the final working equations for g-tensor calculations in the framework of an RMB basis, one may simply substitute Eq. (46) for all occurrences of $\mathbf{X}^{B_u}$ in Sec. III.

VI. COMPUTATIONAL DETAILS

In this work, we shall discuss the components of the g-shift Δg_u, which are defined as the relative change of the g-tensor eigenvalues with respect to the absolute value of the electron spin g-factor, $g_e \approx 2.002\,319$,

Published under an exclusive license by AIP Publishing

$$g_u = g_e + \Delta g_u. \quad (47)$$

The g-tensor eigenvalues g_u are calculated as the square root of the G-tensor eigenvalues, where $\mathbf{G} = \mathbf{g}\mathbf{g}^{\mathsf{T}}$. The sign of the g-tensor eigenvalues is chosen such that the product $g_1 g_2 g_3$ has the same sign as the determinant of the g-tensor (see Refs. 21, 76, and 77). In the present work, all g-tensor determinants are positive; therefore, we have chosen all g-tensor eigenvalues to be positive.

All calculations were performed with a developer's version of the ReSpect program,[17,78] using the Dirac–Kohn–Sham approach, and the nonrelativistic exchange–correlation (xc) functionals PBE,[79–81] PBE0,[79–82] BLYP,[79,83,84] and B3LYP.[79,83–86] Furthermore, the xc potential is formulated within the Kramers-unrestricted noncollinear methodology as specified in Table I in Ref. 32. The numerical integration of the xc potential was done with an adaptive molecular grid of medium size (program default, which is about 10 000 points per atom). In all calculations, we used the Gaussian nuclear charge model[68] and the one-center approximation for the [SS|SS] integral class.[17] We utilized all-electron uncontracted Gaussian-type orbital basis sets of double-ζ, triple-ζ, and quadruple-ζ quality plus versions thereof augmented with various types of additional basis functions. In particular, we employed the basis sets of Dyall that include various additional function-types denoted by small letters: (v) valence correlating and valence dipole polarization functions, (c) core correlating functions, and (a) diffuse (augmenting) functions. In this work, we have used specifically the bases labeled dyall-XZ, dyall-vXZ, dyall-cvXZ, and dyall-acvXZ, where X = D, T, Q.[87–93] In addition, we employed Dunning's cc-pV(X+d)Z basis set for third row elements and cc-pVXZ basis set for the remaining light atoms, both standard and augmented with diffuse functions.[94–98]

In some calculations, we employed the resolution-of-identity approximation for the Coulomb contribution to the Fock matrix (RI-J).[99] In the case of Table III, we used the RI-J technique to speed up the calculation, whereas in the case of Table S5 in the supplementary material, we used RI-J out of necessity as the theory described in Sec. V is implemented in the ReSpect program only in conjunction with the RI-J technique. The auxiliary basis sets for the RI-J procedure were generated by a modified even-tempered algorithm[100] and are part of the latest release of the ReSpect program package version 5.2.0 (see Ref. 78).

The geometry of the trans–trans conformation of *N*-acetylglycyl radical (labeled here as TT-NAG) has been taken from Ref. 101, and the geometry of the Ru(III) anti-tumor metastasis inhibitor, *trans*-(dimethyl sulfoxide)-(imidazole) tetrachlororuthenate(III)[102] (labeled here as NAMI), from Ref. 103. The geometry of 6,6′-[1,2-phenylenebis(azanediyl)] bis(phenolato) tellurate(-1) (labeled here as Te–N anion) has been obtained from Ref. 104 by substituting tBu groups by hydrogen atoms in the crystallographic dataset No. 2005030. The geometry of $[Re_3S_4(H_2PCH_2CH_2PH_2)_3Br_3]^+$ (denoted here as Re_3S_4 cluster)

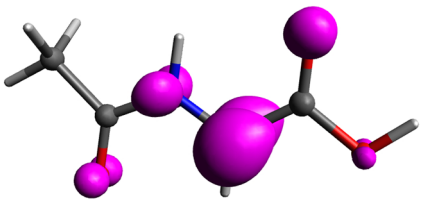

FIG. 1. Isosurface of the spin density magnitude for TT-NAG (value = 0.01 a.u.).

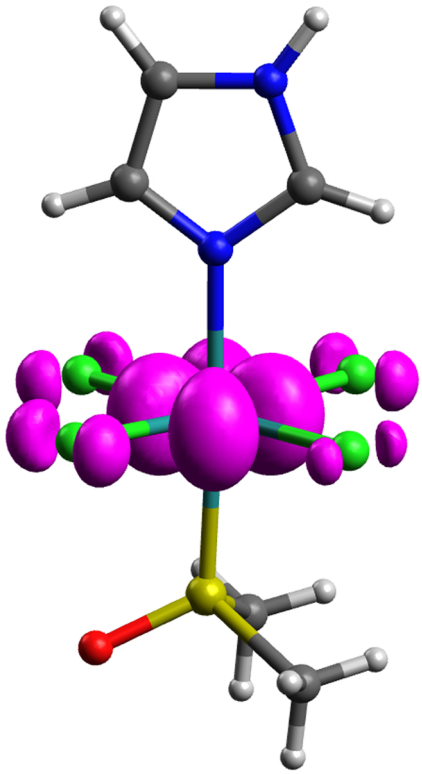

FIG. 2. Isosurface of the spin density magnitude for NAMI (value = 0.005 a.u.).

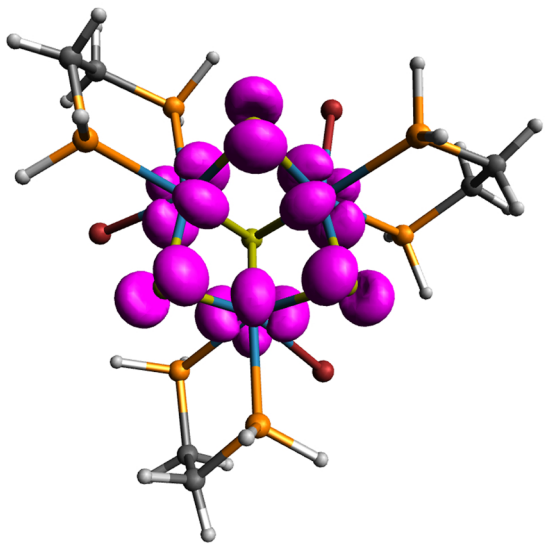

FIG. 3. Isosurface of the spin density magnitude of Re_3S_4 cluster (value = 0.01 a.u.).

Published under an exclusive license by AIP Publishing

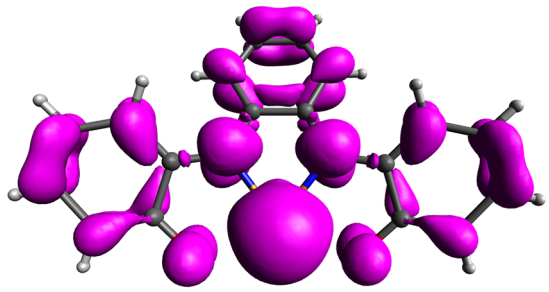

FIG. 4. Isosurface of the spin density magnitude of Te–N anion (value = 0.001 a.u.).

has been taken from Table S2 in the supplementary material of Ref. 105. The orientations of the g-tensor principal axes of Re_3S_4 cluster, Te–N anion, TT-NAG, and NAMI are shown in Figs. S1–S4 in the supplementary material. The geometries for ClO_3, GeH_3, SiH_3, SO_3^-, and MgF have been taken from Ref. 52 and those for TeO, TeS, and Te_2, from Ref. 106. For the SnH_3 molecule, we have used the geometry resulting from the relativistic optimization published in Ref. 55. Finally, the geometries of O_sOF_5 and TiF_3 have been taken from Refs. 11 and 53, respectively.

Note that the visualizations in Figs. 1–4 depict the magnitude of the spin density, as the spin density is a vector field rather than a scalar field when obtained by relativistic methods that include spin–orbit effects.

VII. RESULTS AND DISCUSSION

A. Calculations of the g-tensor using an RMB basis in conjunction with a common gauge origin

In Secs. III–V, we have presented four-component theories for the calculation of the g-tensor based on the RMB–GIAO, RKB, and RMB bases, respectively. The last two approaches depend on the choice of the common gauge origin (CGO); therefore, from now on, we will label them as the RKB–CGO and RMB–CGO methods. The advantage of the RKB–CGO method lies in its computational efficiency (no four-center integrals in a magnetic basis are involved), while RMB–GIAO has superior convergence with the basis set size (see the discussion below). For the purpose of this work, we have also implemented the RMB–CGO method to check whether it has any computational advantage over the RKB–CGO or RMB–GIAO approaches. In Table S1 in the supplementary material, we compare RKB–CGO and RMB–CGO g-shifts using a basis of double-ζ quality, a case in which the differences would be most pronounced. As seen from the table, the differences between the methods are negligible and, thus, the RMB–CGO method provides no computational advantage over the RKB–CGO approach. The insignificance of the effect of including the RMB basis when compared to the RMB–GIAO basis can be understood by the fact that the magnetic part of the RMB basis affects only the small components, while GIAOs influence both the large and small components of the four-component MOs. In the complete basis, the four-component expressions for the first-order magnetic properties (including the g-tensor) depend only on the occupied unperturbed MOs.[60] Therefore, one expects a rather minor effect of the RMB basis, as it affects only the small components of the MOs, which are small in the case of occupied unperturbed MOs. On the other hand, the four-component expressions for the second-order magnetic properties in the complete basis depend on the linear-response MOs.[107] More importantly, the expansion of the linear-response MOs contains vacant unperturbed negative-energy MOs[38,108] for which the small components of the MOs are large. Therefore, an accurate description of the linear-response MOs requires the magnetically balanced basis (see Refs. 37–44), e.g., the RMB basis.[37,39–41] In principle, there could exist situations where the RMB–CGO method has a significantly better convergence with basis set size than the RKB–CGO method. However, the RMB–CGO approach has no significant computational advantage over the superior RMB–GIAO method and, thus, should be abandoned altogether.

In the view of the above discussion, an interesting question is whether the RKB–GIAO basis would yield similar results as RMB–GIAO one and whether it could significantly reduce the computational cost because of the simplified calculation of the two-electron integrals. In Sec. S1 in the supplementary material, we analyze the consequences of the two possible definitions of the RKB–GIAO basis in comparison to the RMB–GIAO one. The key takeaway is that both RKB–GIAO approaches have only a minor computational advantage over the RMB–GIAO approach as the calculation of the time-consuming two-electron integrals over functions of higher cardinal number that originate from the London phase factor, Eq. (16), is necessary in all approaches. In addition, a theoretical analysis reveals the inferiority of the RKB–GIAO methods compared to the RMB–GIAO approach in the estimated error in variational bounds for the total electronic energy and the gauge dependence of the final expressions. We therefore conclude that the RMB–GIAO method is the preferred four-component method of choice for the calculation of the EPR g-tensor.

B. On the use of contracted and uncontracted basis sets

The four-component calculations with the ReSpect program[17] are allowed only with uncontracted bases and hence the conclusions drawn below are valid only for those bases. Table I presents the components of the g-shift for a series of small compounds, including those for which a strong dependence on the gauge origin was found earlier in Ref. 52. Two different choices of CGO, at the center of nuclear charges (COC) and at a point shifted by 10 Å from the COC in all (x, y, and z) directions, yield only minor differences in the results even for the low-quality double-ζ bases. The use of triple-ζ bases further diminishes these differences (see Table S2 in the supplementary material). This finding is in disagreement with the results presented in Ref. 52. This may be explained by the use of different computational protocols in the two works: different hybrid functionals (PBE0 vs B3LYP), four-component treatment vs perturbation theory based on a nonrelativistic ansatz (one-component treatment), and the effect of using uncontracted bases in the four-component calculations. To verify this, we performed additional calculations for GeH_3—a molecule for which, according to Ref. 52, the components of the g-shift significantly depend on the CGO choice. In these calculations, we employed the B3LYP functional and the def2-SVP and def2-TZVP bases as in Ref. 52. We did the calculations at the one-component and four-component levels (see

Published under an exclusive license by AIP Publishing

TABLE I. Calculated components of the g-shift (in ppt) using the PBE0 xc functional, dyall-vDZ basis for Os and Te, cc-pV(D+d)Z for Mg, Si, S, and Cl, and cc-pVDZ for the remaining atoms.

	Gauge	Δg_1	Δg_2	Δg_3
ClO_3	RMB–GIAO[a]	1.254	9.473	9.475
	COC[b]	1.526	10.028	10.029
	COC+10 Å[c]	1.520	9.717	9.722
GeH_3	RMB–GIAO[a]	−1.205	15.977	15.978
	COC[b]	−1.200	15.587	15.589
	COC+10 Å[c]	−1.205	15.170	15.178
MgF	RMB–GIAO[a]	−2.053	−2.053	−0.063
	COC[b]	−2.061	−2.060	−0.053
	COC+10 Å[c]	−1.727	−1.685	−0.011
SiH_3	RMB–GIAO[a]	−0.144	2.332	2.332
	COC[b]	−0.137	2.297	2.298
	COC+10 Å[c]	−0.160	2.661	2.685
SO_3^-	RMB–GIAO[a]	0.266	3.794	3.796
	COC[b]	0.330	3.965	3.968
	COC+10 Å[c]	0.031	5.829	6.129
TeO	RMB–GIAO[a]	−28.860	−28.860	−4.894
	COC[b]	−25.624	−25.624	−4.878
	COC+10 Å[c]	−29.752	−29.459	−4.580
Te_2	RMB–GIAO[a]	−88.832	−88.832	−11.842
	COC[b]	−85.015	−85.015	−11.828
	COC+10 Å[c]	−85.015	−85.015	−11.828
TT-NAG	RMB–GIAO[a]	−0.184	1.748	3.316
	COC[b]	−0.182	1.616	3.125
	COC+10 Å[c]	−0.169	1.487	3.611
$OsOF_5$	RMB–GIAO[a]	−374.500	−374.452	−179.871
	COC[b]	−377.637	−377.587	−188.002
	COC+10 Å[c]	−380.119	−380.034	−187.975

[a]Data calculated using RMB–GIAO basis (see the theory described in Sec. III).
[b]Data calculated using RKB basis (see the theory described in Sec. IV). Gauge origin is placed at the center of nuclear charges (COC).
[c]Data calculated using RKB basis (see the theory described in Sec. IV). Gauge origin is placed at the distance of 10 Å from the COC in each *x*, *y*, and *z* directions.

Tables S3 and S4 in the supplementary material, respectively), where in the one-component calculations, we employed bases in both contracted and uncontracted forms. It turned out that at the one-component level, the use of uncontracted bases dramatically reduces the dependence of the g-shift on the CGO choice compared to the use of contracted bases. Therefore, for small and moderate-sized systems, the use of uncontracted bases may be a good option for the CGO calculation of the EPR g-tensor in the absence of GIAOs.

C. Convergence with the basis set size of the implemented RMB–GIAO method

The first example chosen for the validation of our implementation of the RMB–GIAO approach is the trans–trans conformation of *N*-acetylglycyl (TT-NAG) radical. The EPR parameters of the TT-NAG radical have been studied, and a significant gauge dependence of the g-tensor has been reported.[101]

The structure, the numbering of atoms, and the orientation of the g-tensor principal axis system of TT-NAG are shown in Fig. 5 and Fig. S1 in the supplementary material. As seen in Fig. 1, the distribution of the spin density in this radical is strongly delocalized, which makes it an excellent case study for comparing g-tensors calculated with different choices of gauge origins, see Table II. Besides RMB–GIAO, we also calculated the g-shift components with CGO at the center of nuclear charges (COC) and at different non-hydrogen atoms. The presented results were obtained with the non-augmented triple-ζ basis (cc-pVTZ used in this particular case), which is commonly used as a highest-quality basis set in DFT applications. We also show the difference between the cc-pVTZ results and the results obtained with a significantly larger basis set, augmented cc-pVQZ (both in absolute values and as percentages). As expected, the calculated g-tensors exhibit significant dependence on the choice of gauge origin, though not all components are affected equally. The smallest component Δg_x, perpendicular to the radical plane, shows the weakest dependence. This can be attributed to the nearly symmetric distribution of the spin density along this principal axis (see Fig. 1). In contrast, the spin density along the other two principal axes of the g-tensor in TT-NAG is more delocalized and asymmetric due to the π-system of the radical. Consequently, the y and z principal components are more strongly affected by the choice of gauge origin. For the y component, the difference between the RMB–GIAO value and the value obtained with a particularly bad choice of CGO, at the position of O_3, is above 160 ppm. The placement of the gauge origin at C_α, closer to the maximum of the spin density, also does not bring the calculated Δg_y and Δg_z into satisfactory agreement with the RMB–GIAO values, with a difference of about 100 ppm for Δg_y and 120 ppm for Δg_z. The full results of the g-shift components calculated with cc-pVXZ (X = D, T, Q) basis sets, both the basic and augmented versions, can be found in Tables S5 and S6 in the supplementary material. The convergence of the isotropic g-shift value with basis set quality, as calculated with both RMB–GIAO and RKB–CGO, is shown in Fig. S5 in the supplementary material. As expected, the RMB–GIAO values converge faster than their RKB–CGO counterparts when non-augmented bases are employed. However, in the case of augmented bases, RMB–GIAO and RKB–CGO yield almost identical results (the solid and dashed black lines), though the use of augmented bases in routine applications would be impractical due the increased computational cost involved even with the RKB–CGO method. The addition of core correlating functions to valence bases (labeled as cv

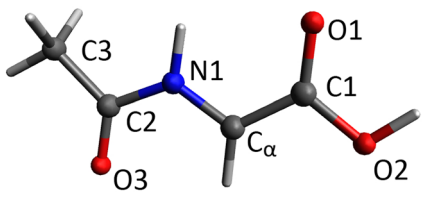

FIG. 5. Atom numbering of TT-NAG.

Published under an exclusive license by AIP Publishing

TABLE II. Calculated components of the g-shift (in ppm) for TT-NAG radical using PBE xc functional and cc-pVTZ basis set, compared with values obtained with augmented cc-pVQZ basis at RMB–GIAO level. Data are calculated using theory that is based either on the RMB–GIAO basis (see Sec. III) or on the RKB basis (see Sec. IV) with various choices of gauge origin.

	Δg_x			Δg_y			Δg_z		
Gauge	cc-pVTZ	Δ[a]	$\Delta_{\%}$[b]	cc-pVTZ	Δ[a]	$\Delta_{\%}$[b]	cc-pVTZ	Δ[a]	$\Delta_{\%}$[b]
RMB–GIAO	−180.8	1.4	0.8	1818.9	−4.6	0.3	3471.3	−0.6	0.0
COC[c]	−183.3	3.9	2.2	1716.3	98.0	5.4	3370.7	100.0	2.9
C_α[d]	−183.4	4.0	2.2	1719.1	95.2	5.2	3352.2	118.5	3.4
C1[d]	−184.4	5.0	2.8	1753.8	60.5	3.3	3345.6	125.1	3.6
C2[d]	−182.2	2.8	1.6	1677.1	137.2	7.6	3396.1	74.6	2.1
C3[d]	−182.0	2.6	1.4	1672.9	141.4	7.8	3434.0	36.7	1.1
O1[d]	−184.9	5.5	3.1	1774.3	40.0	2.2	3368.4	102.3	2.9
O2[d]	−184.7	5.3	3.0	1761.3	53.0	2.9	3312.1	158.6	4.6
O3[d]	−181.7	2.3	1.3	1654.1	160.2	8.8	3376.4	94.3	2.7
N1[d]	−183.1	3.7	2.1	1709.7	104.6	5.8	3385.2	85.5	2.5

[a]Difference between results obtained with augmented cc-pVQZ and cc-pVTZ basis sets, see Tables S5 and S6 in the supplementary material.
[b]Deviation from values obtained with augmented cc-pVQZ basis in %.
[c]Gauge origin placed at the center of nuclear charges (COC) of the molecule.
[d]Gauge origin placed at the specific atom, labeled according to Fig. 5.

and v, respectively) does not change the results, probably because the difference between these bases is insignificant for light elements.

It has been shown that the gauge origin problem in g-tensor calculations may be more severe for larger systems.[52] Moreover, larger systems, especially containing heavy elements, are computationally challenging, especially when using GIAOs at the relativistic four-component level. Therefore, our two next examples are the Te–N anion and Re_3S_4 cluster (see Figs. S2 and S3 in the supplementary material). The Te–N anion is an asymmetric doublet system with highly delocalized spin density (Fig. 4). The Re_3S_4 cluster is a quartet system that contains three metal centers with unpaired electrons and the spin density is symmetrically distributed among Re and three S atoms (Fig. 3). The components of the g-shift were calculated using RMB–GIAO and RKB–CGO with CGO at the center of nuclear charges (see Table III). We used double- and triple-ζ quality valence basis sets (Dyall's on Re and Te and Dunning's on the rest of atoms). The Dyall basis sets were extended by core correlating and diffuse functions, and the Dunning basis sets by diffuse functions and by d functions for P and S (see Sec. VI for more details). The bases of double-ζ quality perform poorly for the Re_3S_4 cluster, which is probably because they are not adequate for the calculation of the g-tensor in the case of strongly delocalized spin density (see columns $\Delta_{\%}$). In both systems in Table III, the effect of adding diffuse functions to the triple-ζ basis is negligible in the RMB–GIAO results, whereas it is still substantial in the RKB–CGO results. Furthermore, the core correlating functions for Te and Re and additional d functions for P and S in the RMB–GIAO calculations have a larger effect on the RMB–GIAO results than diffuse functions. As expected, for both compounds, the RMB–GIAO results converge faster than the RKB–CGO results with increasing quality of the basis set.

Furthermore, we verified the conclusions concerning the convergence of the RMB–GIAO and RKB–CGO results with the size of Dyall's bases, which are specifically designed for relativistic calculations and are in general bigger than standard nonrelativistic basis sets. For this purpose, we plotted the dependence of the isotropic g-shift value on the basis set quality for a series of small compounds (see Figs. S6–S10 in the supplementary material). The calculations were performed with a series of bases, starting with dyall-vXZ (X = D, T, Q) and extending them by adding core correlating and augmenting (diffuse) functions. For educational purposes, we included some results obtained with the dyall-XZ bases (Figs. S7–S10 in the supplementary material). As expected, the absence of valence correlating and valence dipole polarization functions in the basis set has significant negative consequences for the g-tensor calculations. Additionally, we demonstrated the relative errors of the g-shift values calculated with different bases compared to the results obtained with the RMB–GIAO method and dyall-acvQZ basis taken as the basis set limit (see Fig. S11 in the supplementary material). We have also plotted the effect of the basis set quality on the components of the g-shift for the Te–N anion and Re_3S_4 cluster, shown in Figs. S12 and S13, respectively. For all systems, the addition of augmenting functions is more important for the RKB–CGO calculations than for RMB–GIAO because the inclusion of London orbitals extends the basis set with functions with higher angular momentum, thus partially substituting augmenting functions. The use of a double-ζ quality basis set, including its extended forms (up to acvDZ basis), may yield highly unsatisfactory results even with the RMB–GIAO method, e.g., TeO, TeS, and Te_2 in Fig. S11. The RKB–CGO results obtained with extended dyall-acvXZ bases converge almost as well, or just as well, as the RMB–GIAO results. However, the calculations with augmented bases containing diffuse functions with high angular momentum become computationally demanding for moderate-sized systems.

To check the necessity of using diffuse functions, we separated the effects of core correlating and augmenting (diffuse) functions

Published under an exclusive license by AIP Publishing

TABLE III. Calculated components of the g-shift (in ppt) using RKB (CGO) and RMB–GIAO (GIAO) basis. Gauge origin is placed at the center of nuclear charges. The data have been calculated with PBE xc functional and RI-J approximation.

		Δg_x				Δg_y				Δg_z			
		CGO[a]	$\Delta_{\%}$[b]	GIAO[c]	$\Delta_{\%}$[b]	CGO[a]	$\Delta_{\%}$[b]	GIAO[c]	$\Delta_{\%}$[b]	CGO[a]	$\Delta_{\%}$[b]	GIAO[c]	$\Delta_{\%}$[b]
Te–N anion	vDZ[d]	−30.254	−2.3	−30.527	−1.4	14.370	53.2	12.846	37.0	−14.027	−18.4	−16.878	−1.8
	cvDZ[e]	−30.030	−3.0	−30.340	−2.0	13.957	48.8	12.330	31.5	−14.670	−14.6	−17.269	0.5
	acvDZ[f]	−31.022	0.2	−31.404	1.4	8.971	−4.4	9.815	4.6	−18.762	9.2	−18.347	6.8
	vTZ[g]	−30.364	−1.9	−30.398	−1.8	10.498	11.9	10.411	11.0	−14.594	−15.1	−16.411	−4.5
	cvTZ[h]	−30.191	−2.5	−30.234	−2.3	10.006	6.7	9.809	4.6	−15.362	−10.6	−16.905	−1.6
	acvTZ[i]	−30.459	−1.6	−30.956	0.0	8.841	−5.7	9.379	0.0	−17.210	0.2	−17.183	0.0
Re_3S_4 cluster	vDZ[d]	2.341	−75.2	3.300	−65.1	2.853	−70.9	3.834	−60.9	−89.818	7.7	−88.605	6.3
	cvDZ[e]	3.056	−67.7	5.096	−46.1	3.446	−64.9	5.502	−43.9	−87.569	5.0	−85.966	3.1
	acvDZ[f]	5.740	−39.3	5.922	−37.4	6.174	−37.1	6.355	−35.2	−89.931	7.9	−89.992	7.9
	vTZ[g]	8.811	−6.8	8.261	−12.6	9.240	−5.8	8.696	−11.4	−84.300	1.1	−84.413	1.3
	cvTZ[h]	8.673	−8.3	9.244	−2.2	9.068	−7.6	9.647	−1.7	−82.943	−0.5	−82.658	−0.9
	acvTZ[i]	9.615	1.7	9.456	0.0	9.987	1.8	9.810	0.0	−83.243	−0.2	−83.369	−0.0

[a]Data calculated using the theory described in Sec. IV.
[b]Deviation from values obtained with the RMB–GIAO method and acvTZ basis in %.
[c]Data calculated using the theory described in Sec. III.
[d]Basis of double-ζ quality: dyall-vDZ for Te and Re and cc-pVDZ for the remaining atoms.
[e]Basis of double-ζ quality: dyall-cvDZ for Te and Re, cc-pV(D+d)Z for P and S, and cc-pVDZ for the remaining atoms.
[f]Basis of double-ζ quality: dyall-acvDZ for Te, dyall-cvDZ for Re, augmented cc-pV(D+d)Z for P and S, and augmented cc-pVDZ for the remaining atoms.
[g]Basis of triple-ζ quality: dyall-vTZ for Te and Re and cc-pVTZ for the remaining atoms.
[h]Basis of triple-ζ quality: dyall-cvTZ for Te and Re, cc-pV(T+d)Z for P and S, and cc-pVTZ for the remaining atoms.
[i]Basis of triple-ζ quality: dyall-acvTZ for Te, dyall-cvTZ for Re, augmented cc-pV(T+d)Z for P and S, and augmented cc-pVTZ for the remaining atoms.

on the isotropic part of the g-tensor. We compared the relative errors of the results obtained with dyall-avXZ and dyall-cvXZ bases (X = D, T, Q) in Fig. S14 in the supplementary material. It appears that for all the considered systems in Fig. S14 except for TT-NAG (consisting only of light elements), the inclusion of core correlating functions improves the results more than augmenting basis sets with diffuse functions. Moreover, adding augmenting functions to double-ζ bases may worsen the results, e.g., TeO, TeS, and Te_2 in Fig. S14. The role of core correlating functions in calculating the g-tensor can be rationalized as follows: The g-tensor can be primarily viewed as a valence-shell property. However, valence-shell orbitals, being orthogonal to the core orbitals, are affected by spin-polarization of the latter. It was shown that core orbitals of transition metals, in particular 2s and 3s, can be strongly polarized, sometimes even stronger than valence-shell orbitals (see Tables 1 and 2 in Ref. 109). The inclusion of core correlating functions may not be necessary for all atoms (see Tables S8 and S9 in the supplementary material). We have plotted the relative errors of the calculated g-shift components for the Te–N anion and Re_3S_4 cluster (see Figs. S15 and S16 in the supplementary material) when core correlating functions are added to the basis only for selected atoms. It appears that for the Te–N anion, core correlating functions are necessary only for Te (see Fig. S15 in the supplementary material). However, for the Re_3S_4 cluster, core correlating functions on the heavier atoms—Re and Br—do not affect the results (Fig. S16 in the supplementary material, options c1 and c2), whereas they are important for S, dyall-(c3)vXZ basis, and light elements (bases dyall-cvXZ, X = D, Z). Note, that standard nonrelativistic basis sets for light elements may not contain core correlating functions (e.g., cc-pVXZ basis for S). Perhaps, some insight which atoms may need core correlating functions may be obtained by plotting the spin density obtained from a pilot calculation with a relatively small basis set (see Fig. S17 and Fig. 3 showing the spin density in Te–N anion and Re_3S_4 cluster, respectively). From the other side, in terms of computational time, extending basis sets with core correlating functions costs less than with augmenting functions because the latter have higher angular momentum. In conclusion, we recommend to use RMB–GIAO method using basis of triple-ζ quality with core correlating functions added at least for heavy and moderately heavy atoms, where significantly polarized core is expected.

D. Double point-group symmetry considerations

The g-tensor of the planar system TiF_3 exhibits a vanishingly small dependence on the position of the gauge (see columns with $n = 1$ in Table IV). This can be rationalized by using double group theory, which in this case predicts that the integral of the current density, Eq. (42), vanishes even in the finite basis. To prove this statement, it is convenient to express the four-component current density via the MOs, as written in Eq. (A8). Taking time-reversal symmetry into consideration, one can show that the MO pairs that constitute Kramers partners generate current densities with opposite signs. Therefore, from the form of Eq. (A8), it is clear that in the Kramers-restricted methodology, the current density is determined solely by the singly occupied MOs (SOMOs), i.e., by the MOs without occupied Kramers partners. In the Kramers-unrestricted

Published under an exclusive license by AIP Publishing

TABLE IV. Calculated isotropic g-shift for linear clusters of TiF_3, SnH_3, and $OsOF_5$ containing n (1–5) molecules separated by 10 Å in the direction of the symmetry axis of the molecules. All values were calculated using the PBE xc functional, cc-pVDZ basis for light and dyall-vDZ basis for heavy atoms (Sn and Os), and the relativistic theory based on the RKB basis described in Sec. IV.

		COC[b]					COC+20 Å[c]	
	Symmetry[a]	$n = 1$	$n = 2$	$n = 3$	$n = 4$	$n = 5$	$n = 1$	$n = 5$
$[TiF_3]_n$	D_{3h}	−32.39	−32.39	−32.36	−32.35	−32.35	−32.39	−32.35
$[SnH_3]_n$	C_{3v}	21.48	21.47	21.46	21.46	21.46	24.56	24.55
$[OsOF_5]_n$	C_{4v}	−341.43	−341.53	−341.47	−341.43	−341.41	−333.49	−333.67

[a]Point-group symmetry of the molecule.
[b]Gauge origin placed at the center of nuclear charges (COC).
[c]Gauge origin placed 20 Å (two intermolecular distances) away from the COC in the positive direction.

methodology (used in this work), one can still determine approximate Kramers partners as well as the approximate SOMOs that usually give the dominant contribution to the current density. The TiF_3 system belongs to the D_{3h} group, and its SOMO belongs to the $E_{1/2}$ irreducible representation (irrep) of that group. In addition, the Dirac matrices $\vec{\boldsymbol{\alpha}}$ transform under the double point-group operations in the same way as the position vector, and therefore in the case of D_{3h}, the $(\boldsymbol{\alpha}_x, \boldsymbol{\alpha}_y)$ pair and $\boldsymbol{\alpha}_z$ belong to the E' and A_2'' irreducible representations, respectively (here, z is the symmetry axis). The integral of the four-component current density generated by the TiF_3 SOMO then vanishes because neither the direct product $E_{1/2} \otimes E_{1/2} \otimes E'$ nor $E_{1/2} \otimes E_{1/2} \otimes A_2''$ contains the totally symmetric D_{3h} irreducible representation A_1'.

There are two useful points one may further infer from the analysis of molecular symmetry. First, the relative strength of the gauge dependence caused by the different components of the gauge vector may also be deduced from double group theory. For example, analyzing the symmetry of the $OsOF_5$ system reveals that the dominant gauge dependence is along its symmetry axis (because z belongs to the totally symmetric C_{4v} irrep A_1). Second, in many systems containing one heavy element, the SOMOs are often centered on the heavy atom, so it may be useful to analyze the approximate symmetry of the immediate chemical environment of that heavy atom. For example, in NAMI, a compound investigated for its potential in clinical application,[110,111] the weak gauge dependence of the g-tensor results (also studied in Ref. 48) can be explained by double group theory even though the system is not symmetric. The structure of NAMI and the distribution of the spin density are shown in Fig. 2. The components of the g-shift calculated with the RMB–GIAO and RKB–CGO methods for three different CGO choices are presented in Table S7, and the orientation of the g-tensor principal axes is shown in Fig. S4 in the supplementary material. The computations were done with dyall-cvXZ bases (X = D, T, Q). As mentioned above, the gauge dependence of the g-tensor results is small and remains so even for the most extreme choice of the gauge at COC+100 Å (compare with the results for TT-NAG in Table S5 in the supplementary material). One can rationalize this weak dependence as follows: The immediate chemical environment of ruthenium belongs approximately to the C_{4v} group. However, the distribution of the spin density magnitude, Fig. 2, suggests that the SOMO has an approximate symmetry of O_h rather than C_{4v}. Indeed, upon closer analysis, it can be shown that the SOMO approximately belongs to the $F_{3/2g}$ irrep of the O_h group. Because the direct product $F_{3/2g} \otimes F_{3/2g} \otimes T_{1u}$ does not contain the totally symmetric O_h irrep A_{1g}, this part of the SOMO gives a vanishing contribution to the integral of the current density, Eq. (42). Therefore, the weak gauge dependence of the g-tensor results of NAMI is caused only by the smaller, nonsymmetric parts of the SOMO (i.e., by the small deviation of the SOMO from being perfectly O_h-symmetrical) and by spin-polarization effects, i.e., by the remaining occupied MOs (see the discussion above).

E. Molecular-cluster computations

Cluster calculations are used in quantum chemistry as an approximation to full periodic calculations of solids. In some cases, simulating solids by clusters may be the only choice; this is because for calculations of many molecular properties, relativistic methods incorporating periodic boundary conditions are not available. When a cluster is composed of individual molecules with a relatively weak intermolecular interaction, then cluster computations usually provide a fair approximation to full periodic calculations. In the following, we will consider only this type of molecular clusters. As shown above, for some molecular systems, the gauge dependence of the results is so significant that it cannot be mitigated by a suitable choice of common gauge origin. An important question is whether this gauge dependence is a serious issue in molecular-cluster calculations. At first glance, one would expect that the gauge dependence of the results is more severe in cluster than in single molecule calculations. This expectation is based on the following reasoning. First, a cluster generally occupies a much larger space than a single molecule, and it has a highly delocalized spin density. Therefore, whatever the choice of the gauge, there is always a molecule within the cluster that is far from the gauge origin. Second, one would assume that the gauge error arising from a single molecule is additive, and thus, it will increase with the number of the molecules in the cluster. However, this assumption is not correct when one chooses a gauge origin at the center of the cluster, e.g., at the center of the nuclear charges (COC). In this case, the gauge error remains approximately constant regardless of the number of molecules in the cluster (see Table IV). The small changes of the g-shift that occur when varying the size of the cluster (see columns with $n = 1, \ldots, 5$) are due to the interaction of individual molecules within the cluster. The distance between molecules was chosen to be 10 Å to minimize this interaction. The small dependence of the

Published under an exclusive license by AIP Publishing

g-shift of the $[\,TiF_3\,]_n$ system can be rationalized by the negligible gauge dependence of the single TiF_3 molecule, see the discussion in the previous paragraph. However, this argument is not valid for the $[\,SnH_3\,]_n$ and $[\,OsOF_5\,]_n$ systems, which have non-negligible dependence of the g-shift on the gauge position, see columns with $n = 1$ in Table IV. The insensitivity of the g-shift to the size of the cluster when COC is chosen as the gauge origin can be easily understood from Eq. (41), if one neglects the intermolecular interaction. In that case, the current density can be decomposed into n identical current densities $\vec{j}_c$, $\vec{j} = \sum_{c=1}^{n} \vec{j}_c$, one for each molecule in the cluster. Then, Eq. (41) can be reformulated as follows:

$$g_{uv} = -\frac{1}{S}\sum_{c=1}^{n}\left\{\int \left[\vec{r}_c \times \vec{j}_c(\vec{r}_c, \vec{J}_v, 0)\right]_u d^3\vec{r}_c - \left[(\vec{r}_0 - \vec{r}_{0c}) \times \int \vec{j}_c(\vec{r}_c, \vec{J}_v, 0) d^3\vec{r}_c\right]_u\right\}, \tag{48}$$

where we have applied the integration-by-substitution method (also known as change of variables) with $\vec{r}_c = \vec{r} - \vec{r}_{0c}$. Here, the new integration variable $\vec{r}_c$ is the vector relative to the center of the nuclear charges of individual molecules within the cluster, $\vec{r}_{0c}$. Because we have imposed a ferromagnetic state on the cluster, i.e., the spins of the individual molecules are aligned, the effective spin of the cluster has the form $S = nS_1$, with S_1 being the effective spin of a single molecule. In addition, because we have neglected intermolecular interaction and used the COC of the cluster as the common gauge origin $\vec{r}_0$, the second term on the RHS of the equation vanishes and Eq. (48) simplifies to

$$g_{uv} = -\frac{1}{S_1}\int \left[\vec{r}_1 \times \vec{j}_1(\vec{r}_1, \vec{J}_v, 0)\right]_u d^3\vec{r}_1. \tag{49}$$

The reason why the sum of the gauge-dependent terms in Eq. (48) vanishes is because for each molecule within the cluster, there exists another one that has the opposite vector $(\vec{r}_0 - \vec{r}_{0c})$ and, thus, their contributions to the gauge dependence [the second term on the RHS of Eq. (48)] cancel each other. In the case of an odd number n of molecules, there are pairs of molecules with cancelling terms plus a central (unpaired) molecule for which $(\vec{r}_0 - \vec{r}_{0c}) = 0$. As a result, Eq. (49) represents the g-tensor of a single molecule with the gauge origin at its COC and thus it does not depend on the size of the cluster. The small changes between the results for different n in Table IV can be attributed to intermolecular interactions within the cluster, which have been neglected in the derivation of Eq. (49). Therefore, if the gauge origin is placed at the center of the cluster, the gauge error is not cumulative and its magnitude is approximately the same as the gauge error for a single molecule. If the gauge origin is shifted away from the center of the cluster by some Δ, then again the magnitude of the total gauge error is approximately the same as the gauge error for a single molecule with the gauge shifted by Δ from the center of that molecule, see the last two columns in Table IV. One can prove this by simply adding Δ to $\vec{r}_0$ and $\vec{r}_{0c}$ vectors in Eq. (48). Note that, on the basis of these considerations, before doing cluster calculations, it would make sense to first estimate the gauge-related error with the intended basis set for a single molecule as the difference between the results obtained when employing the RMB–GIAO (Sec. III) and RKB–CGO (Sec. IV) methods. Then, if the error is small, one may proceed with cluster calculations using the computationally cheaper methodology involving the RKB basis. This procedure does not account for intermolecular interactions within the cluster, but in principle, it validates the results obtained by the inferior RKB–CGO method when computational demands prohibit the use of a method based on the RMB–GIAO basis.

VIII. SUMMARY AND CONCLUDING REMARKS

In this work, we have presented a four-component Dirac–Kohn–Sham method for calculating the electron paramagnetic resonance g-tensor that takes advantage of both the restricted magnetically balanced (RMB) basis and gauge-including atomic orbitals (GIAO). The developed RMB–GIAO method is based on the Dirac–Coulomb Hamiltonian and thus includes nuclear spin–orbit and spin-same-orbit effects to arbitrary order and strength. Furthermore, the method utilizes a recently developed noncollinear regularized xc potential; so, it is not dependent on the rotation of the Cartesian coordinate axis system and provides increased computational stability when compared to older noncollinear schemes. In order to include the important spin-polarization effects, the method is based on the Kramers-unrestricted Kohn–Sham determinant.

We have demonstrated the generally superior convergence, with regard to the basis set size, of the proposed RMB–GIAO method compared to the method based on the restricted kinetically balanced basis (RKB) with a common gauge origin (CGO). Exceptions to this include small systems and systems with a certain symmetry, i.e., systems for which the choice of gauge origin only has a minor or no effect on the calculated g-tensors. The use of double-ζ quality basis sets, including extended forms thereof, may yield highly unsatisfactory results even when obtained with the RMB–GIAO method. The RKB–CGO results for small systems obtained with bases extended by core correlating and diffuse functions converge almost as well, or just as well, as the RMB–GIAO results. For moderate-sized systems with delocalized spin density, the RKB–CGO results obtained with bases of triple-ζ quality without additional core correlating and diffuse functions may deviate from the RMB–GIAO results up to 15%.

In all the examples considered, the RMB–GIAO results converge monotonically to the basis set limit starting with valence triple-ζ bases. In general, for the RMB–GIAO calculations of the g-tensor, core correlating functions are more important than diffuse functions. The smallest basis set that can be expected to provide sufficiently converged RMB–GIAO results (the relative error below 10%) should be of triple-ζ quality extended by core correlating functions on atoms with a significantly polarized core. Those atoms are not necessarily limited to heavy-atom centers, they may include lighter atoms as well.

Using the formulation of the RKB–CGO method via the current densities, we have shown that the gauge dependence of the g-tensor results vanishes in the basis set limit. In particular, we have proved the validity of the continuity equation within the framework of the DKS theory as well as its connection to the gauge-independent g-tensor results by using the divergence theorem. The key point of the proof is the vanishing integral of the current density in the basis set limit. In addition, we used the formulation of the RKB–CGO method via the current density to show how the double point-group symmetry may be useful in analyzing the gauge dependence of the

Published under an exclusive license by AIP Publishing

g-tensor results. For example, we demonstrated that the gauge independence of the g-tensor of TiF_3 is a consequence of the fact that its SOMO belongs to the $E_{1/2}$ irreducible representation (irrep) of the D_{3h} group. Although NAMI is not a symmetric system, its SOMO belongs (approximately) to the $F_{3/2g}$ irrep of the O_h group, which results in a weak gauge dependence of the calculated g-tensors.

Finally, we have discussed the somewhat surprising result that, in molecular-cluster calculations, the gauge error does not increase on increasing the size of the cluster, if the gauge origin is chosen to be in the center of the cluster. To explain this behavior, we have used the formulation of the RKB–CGO method based on current densities. In this formulation, the gauge-dependent term of an individual molecule within the cluster depends linearly on the integral of the current density and on the relative position of the molecule with respect to the center of the cluster. As a result, one can show that the gauge error of the entire cluster equals the gauge error of a single molecule, if the intermolecular interactions are sufficiently small. However, even in the case of nonvanishing intermolecular interactions, the gauge error is still significantly diminished, and it increases only weakly with increasing size of the cluster.

SUPPLEMENTARY MATERIAL

See the supplementary material for a discussion of the RKB–GIAO method; the orientation of the principal axes of the g-tensor in TT-NAG, Te–N anion, Re_3S_4 cluster, and NAMI systems; a comparison of the RKB–CGO and RMB–CGO methods; the performance of the RMB–GIAO method with various basis sets; and def2-SVP, def2-TZVP, and def2-QZVPPD fitting bases for hydrogen and germanium.

ACKNOWLEDGMENTS

We acknowledge the financial support provided by the Slovak Grant Agencies VEGA and APVV (Contract Nos. 2/0135/21 and APVV-19-0516). This study was also supported by the Operation Program of Integrated Infrastructure for the project, UpScale of Comenius University Capacities and Competence in Research, Development and Innovation, ITMS2014+: 313021BUZ3, co-financed by the European Regional Development Fund. In addition, this project received funding from the European Union's Horizon 2020 research and innovation program under the Marie Skłodowska-Curie Grant Agreement No. 945478. M.R. also acknowledges the support received from the Research Council of Norway through a Centre of Excellence Grant (Grant No. 252569) and a research grant (Grant No. 315822) as well as the use of computational resources provided by UNINETT Sigma2—the National Infrastructure for High Performance Computing and Data Storage in Norway (Grant No. NN4654K). We are thankful to Vladimir G. Malkin for valuable comments and James R. Asher for thorough proofreading.

AUTHOR DECLARATIONS

Conflict of Interest

The authors have no conflicts to disclose.

Author Contributions

Debora Misenkova: Conceptualization (equal); Data curation (equal); Methodology (equal); Software (lead); Validation (equal); Visualization (equal); Writing – original draft (equal); Writing – review & editing (supporting). **Florian Lemken**: Data curation (equal); Methodology (supporting); Validation (equal); Visualization (equal); Writing – original draft (supporting); Writing – review & editing (supporting). **Michal Repisky**: Data curation (supporting); Methodology (supporting); Resources (equal); Software (equal); Validation (supporting); Writing – review & editing (supporting). **Jozef Noga**: Conceptualization (equal); Data curation (supporting); Funding acquisition (equal); Methodology (supporting); Resources (equal); Supervision (supporting); Writing – review & editing (supporting). **Olga L. Malkina**: Conceptualization (equal); Data curation (supporting); Funding acquisition (equal); Methodology (supporting); Supervision (supporting); Validation (supporting); Writing – original draft (equal); Writing – review & editing (equal). **Stanislav Komorovsky**: Conceptualization (lead); Data curation (supporting); Methodology (lead); Resources (equal); Software (equal); Supervision (lead); Validation (equal); Visualization (equal); Writing – original draft (lead); Writing – review & editing (equal).

DATA AVAILABILITY

The data that support the findings of this study are available within the article, its supplementary material, and from the corresponding author upon reasonable request.

APPENDIX A: THE CONTINUITY EQUATION WITHIN THE DHF AND DKS THEORY

To show the validity of the continuity equation and the corresponding definition of the charge and current densities in the framework of the DHF and DKS theories, we start from the equation of motion for the ith occupied molecular orbital $\boldsymbol{\varphi}_i(\vec{r},t)$,

$$i\left(\frac{d\boldsymbol{\varphi}_i}{dt}\right) = \left[c(\vec{\boldsymbol{\alpha}}\cdot\vec{\pi}) + (\boldsymbol{\beta}-\mathbf{I}_4)c^2 + \mathbf{V}(\vec{r},t)\right]\boldsymbol{\varphi}_i, \tag{A1}$$

with $\vec{\pi} = \vec{p} + \frac{1}{c}\vec{A}$ being the mechanical momentum operator. Here and in the following, we use bold font on MOs to indicate that they have a four-component form. The level of theory (DHF or DKS) is specified by the choice of the four-component potential $\mathbf{V}(\vec{r},t)$ (see the discussion of the parameter ξ in Sec. III). By multiplying the left side of Eq. (A1) with $\boldsymbol{\varphi}_i^\dagger$, we get [here and in Eqs. (A3)–(A5), i is not a summation index]

$$i\boldsymbol{\varphi}_i^\dagger\left(\frac{d\boldsymbol{\varphi}_i}{dt}\right) = c\boldsymbol{\varphi}_i^\dagger(\vec{\boldsymbol{\alpha}}\cdot\vec{\pi})\boldsymbol{\varphi}_i + \boldsymbol{\varphi}_i^\dagger(\boldsymbol{\beta}-\mathbf{I}_4)c^2\boldsymbol{\varphi}_i + \boldsymbol{\varphi}_i^\dagger\left[\mathbf{V}(\vec{r},t)\boldsymbol{\varphi}_i\right], \tag{A2}$$

and by subtracting its Hermitian adjoint, we obtain the expression

$$\begin{aligned} i\frac{d}{dt}\left(\boldsymbol{\varphi}_i^\dagger\boldsymbol{\varphi}_i\right) = {} & c\boldsymbol{\varphi}_i^\dagger\left(\vec{\boldsymbol{\alpha}}\cdot\vec{\pi}\,\boldsymbol{\varphi}_i\right) - c\left(\vec{\boldsymbol{\alpha}}\cdot\vec{\pi}\,\boldsymbol{\varphi}_i\right)^\dagger\boldsymbol{\varphi}_i + \boldsymbol{\varphi}_i^\dagger\left[(\boldsymbol{\beta}-\mathbf{I}_4)c^2\boldsymbol{\varphi}_i\right] \\ & - \left[(\boldsymbol{\beta}-\mathbf{I}_4)c^2\boldsymbol{\varphi}_i\right]^\dagger\boldsymbol{\varphi}_i + \boldsymbol{\varphi}_i^\dagger\left[\mathbf{V}(\vec{r},t)\boldsymbol{\varphi}_i\right] - \left[\mathbf{V}(\vec{r},t)\boldsymbol{\varphi}_i\right]^\dagger\boldsymbol{\varphi}_i. \end{aligned} \tag{A3}$$

In contrast to the operators $\vec{\boldsymbol{\alpha}}\cdot\vec{A}$ and $(\boldsymbol{\beta}-\mathbf{I}_4)c^2$, the operator that contains the momentum operator, $\vec{\boldsymbol{\alpha}}\cdot\vec{p}$, is not Hermitian in the

Published under an exclusive license by AIP Publishing

matrix sense [because for the dagger operation used above, it holds that $(\vec{p}\,\boldsymbol{\varphi}_i)^\dagger = -\vec{p}\,\boldsymbol{\varphi}_i^\dagger$].

Therefore, while the third and fourth terms on the RHS of Eq. (A3) vanish, the first two terms yield

$$c\boldsymbol{\varphi}_i^\dagger\left(\vec{\boldsymbol{\alpha}}\cdot\vec{p}\,\boldsymbol{\varphi}_i\right) - c\left(\vec{\boldsymbol{\alpha}}\cdot\vec{p}\,\boldsymbol{\varphi}_i\right)^\dagger\boldsymbol{\varphi}_i = -ic\left[\boldsymbol{\varphi}_i^\dagger\vec{\boldsymbol{\alpha}}\cdot\left(\vec{\nabla}\boldsymbol{\varphi}_i\right) + \left(\vec{\nabla}\,\boldsymbol{\varphi}_i\right)^\dagger\cdot\vec{\boldsymbol{\alpha}}\,\boldsymbol{\varphi}_i\right] = -ic\vec{\nabla}\cdot\left(\boldsymbol{\varphi}_i^\dagger\vec{\boldsymbol{\alpha}}\boldsymbol{\varphi}_i\right). \tag{A4}$$

The last two terms in Eq. (A3) vanish for any local Hermitian potentials, such as the xc potential or Coulomb contribution to the Fock operator. On the other hand, in the case of a nonlocal HF exchange potential, one gets the following expression:

$$\begin{aligned}\boldsymbol{\varphi}_i^\dagger(\vec{r}_1)\left[\mathbf{V}^{\mathrm{ex}}(\vec{r}_1)\boldsymbol{\varphi}_i(\vec{r}_1)\right] - \left[\mathbf{V}^{\mathrm{ex}}(\vec{r}_1)\boldsymbol{\varphi}_i(\vec{r}_1)\right]^\dagger\boldsymbol{\varphi}_i(\vec{r}_1) &= \sum_j\boldsymbol{\varphi}_i^\dagger(\vec{r}_1)\left[\int\frac{\boldsymbol{\varphi}_j^\dagger(\vec{r}_2)\boldsymbol{\varphi}_i(\vec{r}_2)}{|\vec{r}_1-\vec{r}_2|}d^3\vec{r}_2\right]\boldsymbol{\varphi}_j(\vec{r}_1)\\ &\quad - \sum_j\boldsymbol{\varphi}_j^\dagger(\vec{r}_1)\left[\int\frac{\boldsymbol{\varphi}_i^\dagger(\vec{r}_2)\boldsymbol{\varphi}_j(\vec{r}_2)}{|\vec{r}_1-\vec{r}_2|}d^3\vec{r}_2\right]\boldsymbol{\varphi}_i(\vec{r}_1),\end{aligned} \tag{A5}$$

which vanishes only if one performs an additional summation over the occupied index *i*. By collecting Eqs. (A3)–(A5), we get the equation

$$\frac{d}{dt}\left(-\boldsymbol{\varphi}_i^\dagger\boldsymbol{\varphi}_i\right) = -\vec{\nabla}\cdot\left[-c\boldsymbol{\varphi}_i^\dagger\vec{\boldsymbol{\alpha}}\boldsymbol{\varphi}_i\right], \tag{A6}$$

where in the presence of an HF exchange potential, the summation over index *i* is required, while in its absence, this summation is optional, i.e., the equation holds both for the sum and for the individual occupied MOs.

In the DHF or DKS theory, the charge density ρ can be expressed as the sum of molecular orbital contributions,

$$\rho = \sum_i\rho_i = -\sum_i\boldsymbol{\varphi}_i^\dagger\boldsymbol{\varphi}_i. \tag{A7}$$

Here, we have used the physical definition of the charge density of electrons, i.e., that it integrates to the charge of the system, which is equal to the number of electrons multiplied by their charge (−1). We note in passing that the definition of ρ_0 in Eq. (34) gives the number of electrons when integrated and, thus, lacks the minus sign. The continuity equation describes a process of transporting some physical quantity. It sets up a mathematical relation between the charge and the current density of the said quantity. If we assume that the continuity equation is satisfied in the framework of the DHF and DKS theory, and we take the charge density as defined by Eq. (A7), then the four-component current density necessarily has the form

$$\vec{j} = \sum_i\vec{j}_i = -\sum_i\boldsymbol{\varphi}_i^\dagger c\vec{\boldsymbol{\alpha}}\boldsymbol{\varphi}_i. \tag{A8}$$

Then, according to Eq. (A6) and the corresponding discussion, within the framework of pure DFT, $\xi = 0$, the continuity equation holds for the charge and current density of the individual MOs,

$$\frac{d\rho_i}{dt} = -\vec{\nabla}\cdot\vec{j}_i. \tag{A9}$$

If, on the other hand, the HF exchange potential is present in the Fock operator, the continuity equation is satisfied for the total charge and current densities only,

$$\frac{d\rho}{dt} = -\vec{\nabla}\cdot\vec{j}. \tag{A10}$$

APPENDIX B: INTEGRAL OF THE CURRENT DENSITY IN $\mathbb{R}^3$

In this section, we will prove that the integral of the current density vanishes, Eq. (42), when the continuity equation, Eq. (A10), is satisfied,

$$\frac{d\rho}{dt} = -\vec{\nabla}\cdot\vec{j} \quad\Rightarrow\quad \iiint\vec{j}\,d^3\vec{r} = 0. \tag{B1}$$

For a time-independent charge density, $\rho \neq \rho(t)$, the continuity equation gives, for any closed volume $\mathcal{V}$, the following relation:

$$\iiint_{\mathcal{V}}\frac{d\rho}{dt}\,d\mathcal{V} = -\iiint_{\mathcal{V}}\vec{\nabla}\cdot\vec{j}\,d\mathcal{V} = 0. \tag{B2}$$

Application of the divergence theorem (also known as Gauss's theorem) to this expression then leads to the following relation:

$$\iiint_{\mathcal{V}}\vec{\nabla}\cdot\vec{j}\,d\mathcal{V} = \oiint_{\mathcal{S}}\vec{j}\cdot d\vec{\mathcal{S}} = 0, \tag{B3}$$

where $\mathcal{V}$ is a three-dimensional closed volume and $\mathcal{S} = \partial\mathcal{V}$ is its boundary. Let us choose the volume $\mathcal{V}$ to be the upper half of a sphere with radius R, $\mathcal{V} = \{x^2 + y^2 + z^2 \leq R, z \geq 0\}$. The boundary of $\mathcal{V}$ consists of the hemisphere $\mathcal{S}_1 = \{x^2 + y^2 + z^2 = R, z > 0\}$ and the disk in the xy plane $\mathcal{S}_2 = \{x^2 + y^2 \leq R, \quad z = 0\}$. The surface integral in Eq. (B3) then becomes

$$\oiint_{\mathcal{S}}\vec{j}\cdot d\vec{\mathcal{S}} = \oiint_{\mathcal{S}_1}\vec{j}\cdot d\vec{\mathcal{S}}_1 + \oiint_{\mathcal{S}_2}\vec{j}\cdot d\vec{\mathcal{S}}_2 = 0. \tag{B4}$$

When the current density $\vec{j}(\vec{r})$ decreases asymptotically faster than $|\vec{r}|^{-2}$ (which is satisfied in the usual quantum chemical calculations of an isolated molecule), then in the limit $R \to \infty$, the first integral on the right-hand side of Eq. (B4) vanishes. Because the integral over the surface $\mathcal{S} = \mathcal{S}_1 + \mathcal{S}_2$ vanishes as well, Eq. (B4) simplifies to

$$\lim_{R\to\infty}\oiint_{\mathcal{S}_2}\vec{j}\cdot d\vec{\mathcal{S}}_2 = 0. \tag{B5}$$

In the limit $R \to \infty$, the integral over the disk with radius R turns into an integral over the xy plane. Keeping in mind that the orientation of the surface normal points outward of a closed volume, one gets the expression

$$\lim_{R\to\infty}\oiint_{\mathcal{S}_2}\vec{j}\cdot d\vec{\mathcal{S}}_2 = -\iint j_z\,dx\,dy = 0. \tag{B6}$$

Finally, we can rewrite the three-dimensional integral of the current density as follows:

$$\iiint j_z\,d^3\vec{r} = \int\left(\iint j_z\,dy\,dx\right)dz = 0. \tag{B7}$$

Published under an exclusive license by AIP Publishing

A similar result can be obtained for each component of the current density $\vec{j}$ by choosing a different orientation of the closed integration area $\mathcal{V}$. *Q.E.D.*

On the basis of Eq. (A9) and the corresponding discussion, for the pure DFT functionals ($\xi = 0$), one may prove the theorem in Eq. (B1) for individual molecular orbitals,

$$\forall i: \quad \frac{d\rho_i}{dt} = -\vec{\nabla}\cdot\vec{j}_i \quad \Rightarrow \quad \iiint \vec{j}_i \, d^3\vec{r} = 0. \tag{B8}$$

REFERENCES

[1] S. Moon and S. Patchkovskii, in *Calculation of NMR and EPR Parameters. Theory and Applications*, edited by M. Kaupp, M. Bühl, and V. G. Malkin (Wiley VCH, Weinheim, 2004), Chap. 20, pp. 325–338.
[2] W. Van Den Heuvel and A. Soncini, Phys. Rev. Lett. **109**, 073001 (2012).
[3] A. Soncini and W. Van Den Heuvel, J. Chem. Phys. **138**, 021103 (2013).
[4] E. Van Lenthe, P. E. S. Wormer, and A. Van Der Avoird, J. Chem. Phys. **107**, 2488 (1997).
[5] I. Malkin, O. L. Malkina, V. G. Malkin, and M. Kaupp, J. Chem. Phys. **123**, 244103 (2005).
[6] P. Hrobárik, O. L. Malkina, V. G. Malkin, and M. Kaupp, Chem. Phys. **356**, 229 (2009).
[7] P. Hrobárik, M. Repiský, S. Komorovský, V. Hrobáriková, and M. Kaupp, Theor. Chem. Acc. **129**, 715 (2011).
[8] J. Autschbach and B. Pritchard, Theor. Chem. Acc. **129**, 453 (2011).
[9] P. Verma and J. Autschbach, J. Chem. Theory Comput. **9**, 1052 (2013).
[10] J. Autschbach, Philos. Trans. R. Soc., A **372**, 20120489 (2014).
[11] S. Gohr, P. Hrobárik, M. Repiský, S. Komorovský, K. Ruud, and M. Kaupp, J. Phys. Chem. A **119**, 12892 (2015).
[12] H. Bolvin and J. Autschbach, *Relativistic Methods for Calculating Electron Paramagnetic Resonance (EPR) Parameters* (Springer Berlin Heidelberg, 2016), pp. 725–763.
[13] R. D. Remigio, M. Repisky, S. Komorovsky, P. Hrobarik, L. Frediani, and K. Ruud, Mol. Phys. **115**, 214 (2017).
[14] J. Novotný, D. Přichystal, M. Sojka, S. Komorovsky, M. Nečas, and R. Marek, Inorg. Chem. **57**, 641 (2018).
[15] P. L. Bora, J. Novotný, K. Ruud, S. Komorovsky, and R. Marek, J. Chem. Theory Comput. **15**, 201 (2019).
[16] A. Wodyński and M. Kaupp, J. Phys. Chem. A **123**, 5660 (2019).
[17] M. Repisky, S. Komorovsky, M. Kadek, L. Konecny, U. Ekström, E. Malkin, M. Kaupp, K. Ruud, O. L. Malkina, and V. G. Malkin, J. Chem. Phys. **152**, 184101 (2020).
[18] Y. J. Franzke and J. M. Yu, J. Chem. Theory Comput. **18**, 2246 (2022).
[19] K. G. Dyall and K. Faegri, Jr., in *Introduction to Relativistic Quantum Chemistry* (Oxford University Press, New York, 2007), Chap. 17, pp. 322–355.
[20] O. L. Malkina, J. Vaara, B. Schimmelpfennig, M. Munzarová, V. G. Malkin, and M. Kaupp, J. Am. Chem. Soc. **122**, 9206 (2000).
[21] S. Komorovsky, in *Relativistic Effects and The Chemistry of Heavy Elements: Relativistic Theory of EPR and (p)NMR*, edited by K. Ruud (Elsevier, 2022).
[22] J. S. Griffith, Mol. Phys. **3**, 79 (1960).
[23] F. G. Eich and E. K. U. Gross, Phys. Rev. Lett. **111**, 156401 (2013).
[24] F. G. Eich, S. Pittalis, and G. Vignale, Phys. Rev. B **88**, 245102 (2013).
[25] D. Gontier, Phys. Rev. Lett. **111**, 153001 (2013).
[26] E. I. Tellgren, Phys. Rev. A **97**, 022513 (2018).
[27] E. Trushin and A. Görling, Phys. Rev. B **98**, 205137 (2018).
[28] J. Kubler, K.-H. Hock, J. Sticht, and A. R. Williams, J. Phys. F: Met. Phys. **18**, 469 (1988).
[29] L. M. Sandratskii, Adv. Phys. **47**, 91 (1998).
[30] C. van Wüllen, J. Comput. Chem. **23**, 779 (2002).
[31] G. Scalmani and M. J. Frisch, J. Chem. Theory Comput. **8**, 2193 (2012).
[32] S. Komorovsky, P. J. Cherry, and M. Repisky, J. Chem. Phys. **151**, 184111 (2019).
[33] J. K. Desmarais, S. Komorovsky, J.-P. Flament, and A. Erba, J. Chem. Phys. **154**, 204110 (2021).
[34] P. Verma and J. Autschbach, J. Chem. Theory Comput. **9**, 1932 (2013).
[35] F. London, J. Phys. Radium **8**, 397 (1937).
[36] R. Ditchfield, J. Chem. Phys. **65**, 3123 (1976).
[37] S. Komorovský, M. Repiský, O. L. Malkina, and V. G. Malkin, J. Chem. Phys. **132**, 154101 (2010).
[38] W. Kutzelnigg, Phys. Rev. A **67**, 032109 (2003).
[39] S. Komorovský, M. Repiský, O. L. Malkina, V. G. Malkin, I. Malkin Ondík, and M. Kaupp, J. Chem. Phys. **128**, 104101 (2008).
[40] L. Cheng, Y. Xiao, and W. Liu, J. Chem. Phys. **131**, 244113 (2009).
[41] M. Repiský, S. Komorovský, O. L. Malkina, and V. G. Malkin, Chem. Phys. **356**, 236 (2009).
[42] M. Olejniczak, R. Bast, T. Saue, and M. Pecul, J. Chem. Phys. **136**, 014108 (2012).
[43] M. Iliaš, H. J. A. Jensen, R. Bast, and T. Saue, Mol. Phys. **111**, 1373 (2013).
[44] M. Repisky, S. Komorovsky, R. Bast, and K. Ruud, in *Gas Phase NMR*, edited by K. Jackowski and M. Jaszuński (The Royal Society of Chemistry, 2016), Chap. 8, pp. 267–303.
[45] G. H. Lushington and F. Grein, Theor. Chim. Acta **93**, 259 (1996).
[46] P. J. Bruna, G. H. Lushington, and F. Grein, Chem. Phys. **225**, 1 (1997).
[47] D. Jayatilaka, J. Chem. Phys. **108**, 7587 (1998).
[48] S. Komorovsky, M. Repisky, K. Ruud, O. L. Malkina, and V. G. Malkin, J. Phys. Chem. A **117**, 14209 (2013).
[49] G. H. Lushington, P. Bündgen, and F. Grein, Int. J. Quantum Chem. **55**, 377 (1995).
[50] M. Kaupp, T. Gress, R. Reviakine, O. L. Malkina, and V. G. Malkin, J. Phys. Chem. B **107**, 331 (2003).
[51] S. Patchkovskii, R. T. Strong, C. J. Pickard, and S. Un, J. Chem. Phys. **122**, 214101 (2005).
[52] M. Glasbrenner, S. Vogler, and C. Ochsenfeld, J. Chem. Phys. **148**, 214101 (2018).
[53] A. Mondal, M. W. Gaultois, A. J. Pell, M. Iannuzzi, C. P. Grey, J. Hutter, and M. Kaupp, J. Chem. Theory Comput. **14**, 377 (2017).
[54] *Calculation of NMR and EPR Parameters. Theory and Applications*, edited by M. Kaupp, M. Bühl, and V. G. Malkin (Wiley VCH, Weinheim, 2004).
[55] G. Schreckenbach and T. Ziegler, J. Phys. Chem. A **101**, 3388 (1997).
[56] F. Neese, J. Chem. Phys. **115**, 11080 (2001).
[57] P. Manninen, J. Vaara, and K. Ruud, J. Chem. Phys. **121**, 1258 (2004).
[58] Z. Rinkevicius, K. J. de Almeida, C. I. Oprea, O. Vahtras, H. Ågren, and K. Ruud, J. Chem. Theory Comput. **4**, 1810 (2008).
[59] B. Sandhoefer and F. Neese, J. Chem. Phys. **137**, 094102 (2012).
[60] M. Repiský, S. Komorovský, E. Malkin, O. L. Malkina, and V. G. Malkin, Chem. Phys. Lett. **488**, 94 (2010).
[61] B. A. Heß, C. M. Marian, U. Wahlgren, and O. Gropen, Chem. Phys. Lett. **251**, 365 (1996).
[62] B. Schimmelpfennig, AMFI, an Atomic Mean-Field Integral Program, 1996.
[63] J. C. Boettger, Phys. Rev. B **62**, 7809 (2000).
[64] M. Filatov, W. Zou, and D. Cremer, J. Chem. Phys. **139**, 014106 (2013).
[65] J. E. Peralta, G. E. Scuseria, and M. J. Frisch, Phys. Rev. B **75**, 125119 (2007).
[66] M. K. Armbruster, F. Weigend, C. van Wüllen, and W. Klopper, Phys. Chem. Chem. Phys. **10**, 1748 (2008).
[67] L. F. Chibotaru, *Advances in Chemical Physics* (John Wiley & Sons, 2013), pp. 397–519.
[68] L. Visscher and K. G. Dyall, At. Data Nucl. Data Tables **67**, 207 (1997).
[69] A. J. Thorvaldsen, K. Ruud, K. Kristensen, P. Jørgensen, and S. Coriani, J. Chem. Phys. **129**, 214108 (2008).
[70] O. Christiansen, P. Jørgensen, and C. Hättig, Int. J. Quantum Chem. **68**, 1 (1998).
[71] R. E. Stanton and S. Havriliak, J. Chem. Phys. **81**, 1910 (1984).
[72] W. Kutzelnigg, Int. J. Quantum Chem. **25**, 107 (1984).
[73] Y. Xiao, W. Liu, L. Cheng, and D. Peng, J. Chem. Phys. **126**, 214101 (2007).
[74] R. Bast, J. Jusélius, and T. Saue, Chem. Phys. **356**, 187 (2009).

Published under an exclusive license by AIP Publishing

[75]S. Komorovsky, K. Jakubowska, P. Świder, M. Repisky, and M. Jaszuński, J. Phys. Chem. A **124**, 5157 (2020).
[76]M. H. L. Pryce, Phys. Rev. Lett. **3**, 375 (1959).
[77]L. F. Chibotaru and L. Ungur, J. Chem. Phys. **137**, 064112 (2012).
[78]ReSpect, version 5.2.0 (2022), Relativistic Spectroscopy DFT program of authors M. Repisky, S. Komorovsky, V. G. Malkin, O. L. Malkina, M. Kaupp, and K. Ruud, with contributions from R. Bast, U. Ekström, M. Hrdá, M. Kadek, S. Knecht, L. Konecny, A. Křístková, E. Malkin, I. Malkin-Ondik, D. Misenkova, and R. Di Remigio. See www.respectprogram.org; accessed on 9 June 2022.
[79]J. C. Slater, Phys. Rev. **81**, 385 (1951).
[80]J. P. Perdew, K. Burke, and M. Ernzerhof, Phys. Rev. Lett. **77**, 3865 (1996).
[81]J. P. Perdew, K. Burke, and M. Ernzerhof, Phys. Rev. Lett. **78**, 1396 (1997).
[82]C. Adamo and V. Barone, J. Chem. Phys. **110**, 6158 (1999).
[83]A. D. Becke, Phys. Rev. A **38**, 3098 (1988).
[84]C. Lee, W. Yang, and R. G. Parr, Phys. Rev. B **37**, 785 (1988).
[85]S. H. Vosko, L. Wilk, and M. Nusair, Can. J. Phys. **58**, 1200 (1980).
[86]P. J. Stephens, F. J. Devlin, C. F. Chabalowski, and M. J. Frisch, J. Phys. Chem. **98**, 11623 (1994).
[87]K. G. Dyall, Basis available from the website, http://dirac.chem.sdu.dk.
[88]K. G. Dyall, Theor. Chem. Acc. **117**, 483 (2007).
[89]K. G. Dyall, Theor. Chem. Acc. **112**, 403 (2004).
[90]K. G. Dyall and A. S. P. Gomes, Theor. Chem. Acc. **125**, 97 (2010).
[91]K. G. Dyall, Theor. Chem. Acc. **99**, 366 (1998).
[92]K. G. Dyall, Theor. Chem. Acc. **108**, 335 (2002).
[93]K. G. Dyall, Theor. Chem. Acc. **115**, 441 (2006).
[94]T. H. Dunning, J. Chem. Phys. **90**, 1007 (1989).
[95]D. E. Woon and T. H. Dunning, J. Chem. Phys. **98**, 1358 (1993).
[96]A. K. Wilson, D. E. Woon, K. A. Peterson, and T. H. Dunning, J. Chem. Phys. **110**, 7667 (1999).
[97]B. P. Prascher, D. E. Woon, K. A. Peterson, T. H. Dunning, and A. K. Wilson, Theor. Chem. Acc. **128**, 69 (2011).
[98]T. H. Dunning, K. A. Peterson, and A. K. Wilson, J. Chem. Phys. **114**, 9244 (2001).
[99]L. Konecny, M. Kadek, S. Komorovsky, K. Ruud, and M. Repisky, J. Chem. Phys. **149**, 204104 (2018).
[100]E. Malkin, M. Repiský, S. Komorovský, P. Mach, O. L. Malkina, and V. G. Malkin, J. Chem. Phys. **134**, 044111 (2011).
[101]S. Kacprzak, R. Reviakine, and M. Kaupp, J. Phys. Chem. B **111**, 811 (2007).
[102]E. Alessio, G. Balducci, A. Lutman, G. Mestroni, M. Calligaris, and W. M. Attia, Inorg. Chim. Acta **203**, 205 (1993).
[103]F. Rastrelli and A. Bagno, Magn. Reson. Chem. **48**, S132 (2010).
[104]P. A. Petrov, E. M. Kadilenko, T. S. Sukhikh, I. V. Eltsov, A. L. Gushchin, V. A. Nadolinny, M. N. Sokolov, and N. P. Gritsan, Chem. - Eur. J. **26**, 14688 (2020).
[105]P. A. Petrov, A. V. Virovets, A. S. Bogomyakov, R. Llusar, C. J. Gómez-García, V. Polo, and S. N. Konchenko, Chem. Commun. **48**, 2713 (2012).
[106]J.-B. Rota, S. Knecht, T. Fleig, D. Ganyushin, T. Saue, F. Neese, and H. Bolvin, J. Chem. Phys. **135**, 114106 (2011).
[107]L. Visscher, T. Enevoldsen, T. Saue, H. J. A. Jensen, and J. Oddershede, J. Comput. Chem. **20**, 1262 (1999).
[108]G. A. Aucar, T. Saue, L. Visscher, and H. J. A. Jensen, J. Chem. Phys. **110**, 6208 (1999).
[109]M. L. Munzarová, P. Kubáček, and M. Kaupp, J. Am. Chem. Soc. **122**, 11900 (2000).
[110]Y. Liu, N. J. Agrawal, and R. Radhakrishnan, J. Mol. Model. **19**, 371 (2012).
[111]M. Oszajca, B. Mrugała, and M. Brindell, Inorg. Chim. Acta **460**, 119 (2017).

Published under an exclusive license by AIP Publishing